chemosensors

MDPI

Review

Two-Dimensional Zinc Oxide Nanostructures for Gas Sensor Applications

Salvatore Gianluca Leonardi

Department of Engineering, University of Messina, c.da di Dio, 98166 Messina, Italy; leonardis@unime.it; Tel.: +39-090-397-7269

Academic Editor: Igor Medintz
Received: 13 April 2017; Accepted: 19 May 2017; Published: 26 May 2017

Abstract: Two-dimensional (2D) nanomaterials, due to their unique physical and chemical properties, are showing great potential in catalysis and electronic/optoelectronic devices. Moreover, thanks to the high surface to volume ratio, 2D materials provide a large specific surface area for the adsorption of molecules, making them efficient in chemical sensing applications. ZnO, owing to its many advantages such as high sensitivity, stability, and low cost, has been one of the most investigated materials for gas sensing. Many ZnO nanostructures have been used to fabricate efficient gas sensors for the detection of various hazardous and toxic gases. This review summarizes most of the research articles focused on the investigation of 2D ZnO structures including nanosheets, nanowalls, nanoflakes, nanoplates, nanodisks, and hierarchically assembled nanostructures as a sensitive material for conductometric gas sensors. The synthesis of the materials and the sensing performances such as sensitivity, selectivity, response, and recovery times as well as the main influencing factors are summarized for each work. Moreover, the effect of mainly exposed crystal facets of the nanostructures on sensitivity towards different gases is also discussed.

Keywords: two-dimensional; zinc oxide; ZnO; nanostructures; gas sensors

1. Introduction

Owing to increasing widespread use in common applications such as industrial production, automotive, medicine, indoor air quality control, and environmental monitoring, gas-sensing technology is receiving more and more attention from both industry and academic research [1]. The increased demand for highly sensitive, selective, cheap, low-power, reliable, stable, and portable sensors has stimulated extensive research to develop new sensing materials. Semiconducting metal oxides have long been considered promising candidates for gas-sensing applications because of their high sensitivity, easy fabrication methods, low cost, and high compatibility with other parts and processes [2–4]. Different types of metal oxide such as ZnO, SnO_2, TiO_2, In_2O_3, WO_3, TeO_2, CuO, CdO, Fe_2O_3, and MoO_3 have been developed and employed in the fabrication of gas sensors and it was found that chemical components, surface state, morphology, and microstructure play important roles in gas-sensing performance [5]. In particular, by reducing the structural dimensions to a few nanometers the surface to volume ratio is extremely increased; therefore, a large active area is provided for the interaction with the gas. Increasing the number of gas molecules adsorbed on the nanostructure leads to a strong improvement of the sensitivity.

Among various nanostructures, one-dimensional (1D) metal oxides have attracted much attention because of their potential excellent sensing performance as well as good chemical and thermal stabilities [6,7]. However, inspired by the superior performance of graphene, the first two-dimensional (2D) material, a lot of research effort has been devoted to the synthesis of other 2D materials [8]. This new class of nanostructures, consisting of one or a few layers of atomic planes, thanks to

their fascinating properties, are showing potentialities in catalysis, electronic, optoelectronic, high performance electrodes, nanocomposites, and sensors [9]. Moreover, due to the high surface to volume ratio, 2D materials provide a large specific surface area and numerous active sites for gas adsorption, which, along with the fast charge transfer ability and tunable chemical and physical properties with the thickness, make these materials efficient in chemical sensing applications. Therefore, 2D materials can be included among the best candidates for the fabrication of ultrahigh sensitive and low-power gas sensor platforms [8,10].

Zinc oxide (ZnO), an n-type semiconductor with a wide bandgap of 3.37 eV, because of its unique optical and electronic properties, in addition to attracting considerable attention in potential applications such as solar cells, optoelectronic devices, nanogenerators, and catalysts [11], has been one of the most investigated sensitive materials for gas sensors [12]. Indeed, due to its advantages of high sensitivity, stability, and low cost, ZnO nanostructures have been widely used for detecting gases such as H_2, NH_3, CH_4, CO, NO_2 ethanol, and acetone [13–18]. Recently, different 2D ZnO nanostructures with thickness close to the space charge region and different exposed facets have been synthesized and employed. The synergic combination of the excellent sensing performance of ZnO with the potentiality of 2D nanostructures has resulted in high detection efficiencies, lowering of operating temperature, fast response and recovery capability, and improvement of the selectivity [19].

This review article presents recent developments in the area of gas sensors where 2D ZnO nanostructures such as nanosheets, nanowalls, nanoflakes, nanoplates, and nanodisks were employed as sensing materials. The synthesis of the material and the sensing performance such as sensitivity, selectivity, response, and recovery times as well as the effect of different exposed facets of ZnO are discussed.

2. ZnO Exposed Crystal Planes and Sensing Behavior

It is well known that the sensitivity strongly depends upon the morphology of metal oxides nanostructure. Therefore, many efforts have been devoted to the synthesis of ZnO nanostructures including quantum nanoparticles [20] nanorods [21], nanofibers [22], nanotubes [23], and three-dimensional (3D), hierarchical nanostructures [24]. However, most of them aimed at an investigation of the effects of morphology and crystal size on the sensing behavior but not on the exploration of their crystal plane-dependent properties. Indeed, theoretical and experimental results indicate that nanostructured materials with exposed crystal surfaces can exhibit special features in applications such as catalysts [25,26] and gas sensors [19,27–30]. Han et al. [31] showed that SnO_2 octahedral nanoparticles with exposed high energy {221} facets, exhibited better gas-sensing performance towards ethanol than those with mainly exposed {110} facets. Similarly, in another work [32], they reported that monodisperse WO_3 nanoparticles with a higher percentage of (010) exposed facets exhibited better gas sensing of 1-butylamine than nanoparticles with (001) and (100) exposed facets.

Yang et al. [33] found that a hierarchical TiO_2 hollow microsphere with exposed high energy {001} crystal facets exhibited enhanced acetone sensing properties compared to hollow and solid microspheres without (001) crystal facets. they further suggested that the (001) surface was highly reactive for the adsorption of active oxygen species, which was responsible for the enhanced sensing performance. As regards ZnO, the dominating exposed crystal facets of these nanostructures are usually $\{10\bar{1}0\}$, because of the natural instinct of ZnO nanocrystals to grow along the c-axis direction [34]. Although it is difficult to synthesize ZnO with unconventional growth directions, it is possible that a particular synthesis method could make it happen. Therefore, materials with similar morphology and specific surface area can be quite different in terms of surface reactivity. Consequently, many studies neglect the effect of exposed reactive surface of ZnO on its sensing properties.

ZnO has many different structural forms; however, wurtzite, a hexagonal structure (space group C6mc) with lattice parameters a = 0.3296 and c = 0.52065 nm, is the most common form of ZnO. The wurtzite structure is made of alternating planes composed of tetrahedrally coordinated O^{2-} and Zn^{2+} ions, stacked along the c-axis. The basal (0001) and $(000\bar{1})$ planes exhibit different bulk

terminations with the first one terminated by positive Zn charges and the second one by negative O charges. As a consequence of these polar surfaces, ZnO shows normal dipole moment and spontaneous polarization along the *c*-axis [35].

Commonly, ZnO has three types of fast growth directions <$2\bar{1}\bar{1}0$> ($\pm[2\bar{1}\bar{1}0]$, $\pm[\bar{1}2\bar{1}0]$, $\pm[\bar{1}\bar{1}20]$), <$01\bar{1}0$> ($\pm[01\bar{1}0]$, $\pm[10\bar{1}0]$, $\pm[1\bar{1}00]$) and $\pm[0001]$ [36]. Intrinsically, due to the higher energy of the (0001) crystal surface than other planes, as mentioned above, the ZnO crystals have a strong tendency to grow along the [0001] direction or the *c*-axis. However, by tuning the growth rates along these directions, a wide range of morphologies with predominate crystal facets can be obtained (Figure 1).

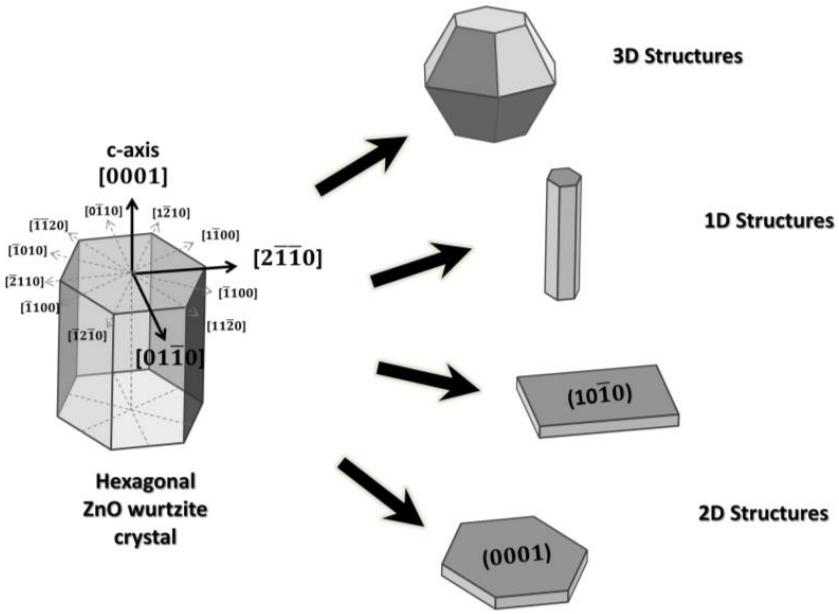

Figure 1. Preferential growth directions of ZnO wurtzite crystal and possible structures.

The hydrothermal method has been widely used as an easy approach to synthesize 2D ZnO nanostructures. It consists of the calcination of intermediates from acetate zinc hydroxyl or hydroxide zinc carbonate salts in order to obtain the ZnO phase [37]. Generally, the formation of nanostructures with preferential crystallographic orientations, then with different exposed facets, is obtained by controlling synthesis conditions such as temperature, the alkalinity of the solution, and the use of surfactants. In particular, specific ionic species can preferentially adsorb onto the plane (0001), stabilizing the surface charge. As a result, the growth along the direction [0001] is greatly suppressed, while the rates of crystal growth along the lateral directions are faster, with consequent formation of two-dimensional structures [11,38].

It is known that in the bulk of wurtzite ZnO, Zn atoms are 4-fold coordinated with O atoms. However, on the surfaces of the crystal, Zn atoms are unsaturated due to the lower coordination number. Because each exposed surface has a specific coordination, a different number of dangling bonds can be found for each crystal facet. The more dangling bonds are present on the exposed crystal surface, the higher the number of oxygen vacancies that can be supplies with adsorption of ionized active species coming from the surrounding environment. These, reacting with electrons from the conduction band, lead to an alteration of the electronic properties of the material. Because the absorption of active species on crystalline surfaces is related to energy aspects, the higher the reduction of energy, the stronger will be the chemisorption of molecules. Therefore, a higher number of dangling bonds can result in an improvement of the sensing performance of the material [34].

In order to understand the effect of different exposed crystal facets, some theoretical studies concerning the adsorption of gas on different reactive surfaces were presented. For instance, Breedon et al. [39,40] studied the adsorption of NO and NO_2 on the ($2\bar{1}\bar{1}0$) crystal face of ZnO by the density functional theory

(DFT) method. they found a weak adsorption on the stoichiometrically balanced surface, although a transfer of charge from the surface to the adsorbed molecule occurred. On the contrary, in the presence of a non-stoichiometric surface, where oxygen vacancies exist, the NO_2 adsorption energy was greater and the magnitude of the charge transfer was calculated to be approximately six times higher than the non-defect surface. Prades et al. [41], by the DFT method, studied the NO_2 and SO_2 chemisorption onto non-polar ZnO $(10\bar{1}0)$ and $(11\bar{2}0)$ surfaces. they found that NO_2 adsorption takes place spontaneously on the stoichiometric and slightly reduced terminations of both non-polar surfaces examined. However, on both surfaces, SO_2 adsorbs more avidly, competing with NO_2 for the same adsorption sites. Yuan et al. [42] used the DFT method to explore the adsorption of different reducing gases onto the $(10\bar{1}0)$ surface of ZnO. Based on their calculations, they proposed that both surface reconstruction and charge transfer resulted in a change of electronic conductance of ZnO. Moreover, analyzing the interactions of different molecules with the exposed surface, they proposed a correlation between the carrier concentration of the ZnO surface and sensitivity.

Therefore, all these findings can be useful for designing novel nanostructures with specifically exposed crystal planes, in order to develop gas sensors with tuned sensing performances.

3. Gas Sensors Based on 2D ZnO Nanostructures

3.1. Volatile Organic Compounds

Volatile organic compounds (VOCs) are a class of organic compounds that, due to their low boiling points, are easily detectable as vapors. they are released in the atmosphere by many anthropogenic sources including transportation, industrial processing, biomass burning, organic solvent, and natural sources such as microbial production and emissions from vegetation [43]. Concentrations of VOCs are much higher indoors compared to outdoors because a wide range of consumer and personal care products, during their use, can release significant amounts of VOCs into the air. Therefore, in addition to CO_2 level, VOCs concentration is used as a parameter to establish the air quality in an indoor environment [44,45].

The monitoring of VOCs by nanostructured metal-oxide-based sensors has been widely investigated and many of them have proven to be effective for this purpose. Among them, ZnO has been one of the best performing sensitive materials for the detection of different species including ethanol, acetone, formaldehyde, acetylene, toluene, benzene, and n-butanol [46]. For this reason, most of the works related to 2D ZnO have been aimed at the investigation of the sensing properties and the development of conductometric sensors for the monitoring of VOCs.

3.1.1. Ethanol

Liu et al. [29] reported a simple gas-phase process to synthesize 3D hierarchical nanostructure based on ZnO nanowhiskers. By the adopted method it was possible, through controlling the ZnO growth along $[10\bar{1}0]$ direction, to grow nanowhiskers with exposed reactive {0001} facets. These nanowhiskers, self-assembling to form ZnO hollow spheres, stabilized the materials against agglomeration (Figure 2a–c). Comparing the ethanol sensing responses of such structures with typical [0001] grown ZnO nanowires, a great enhancement of gas sensitivities for ZnO nanowhiskers based material was observed (Figure 2d). It was also shown by calculation of the chemisorption energy of oxygen, that reactive {0001} facets energetically favored the chemisorption of oxygen species, which enhanced ethanol sensing properties compared to ZnO nanowires, which exhibited $\{10\bar{1}0\}$ side surfaces.

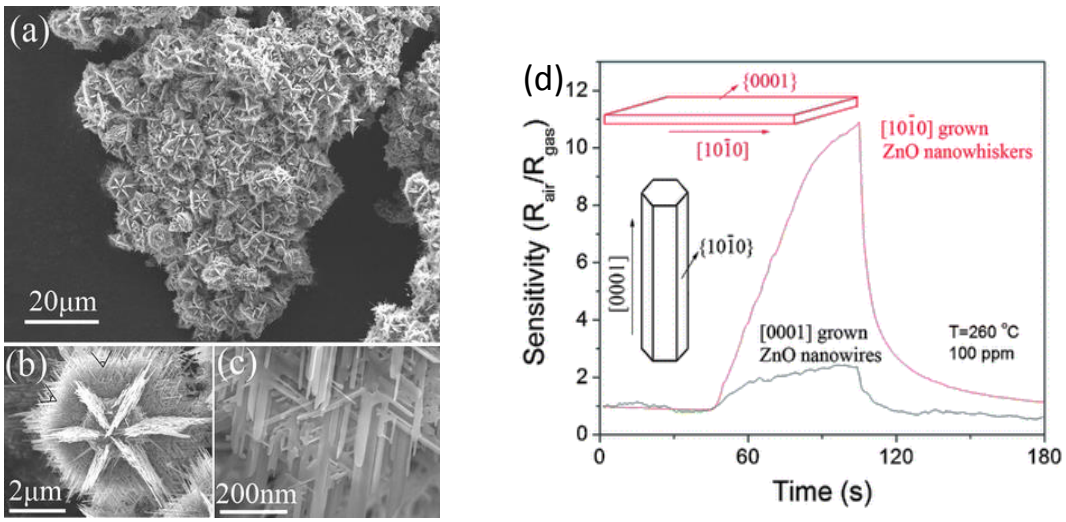

Figure 2. SEM images of ZnO hierarchical nanostructures: (**a**) overall view; (**b**) top view; (**c**) enlarged image of nanobelts; (**d**) comparison of the response to 100 ppm of ethanol gas at 260 °C, between ZnO nanowhisker arrays and typical [0001] grown ZnO nanowires. Reproduced from [29] with the permission of the Royal Society of Chemistry.

Similarly to the previous work, Kaneti et al. [11] demonstrated the strong dependence of the ZnO crystal facets exposed to the gas on the sensing performance. Both ZnO nanoplates and nanorods with exposed (0001) and (10$\bar{1}$0) crystal surfaces, respectively, were synthesized through facile solvothermal methods. ZnO products were mixed with polyvinylidene fluoride (PVDF) and 1-methyl-2-pyrollidone to prepare a paste, then spread onto an alumina ceramic tube with a pair of previously printed Au electrodes. The coated ceramic tube was subsequently aged at 450 °C to improve the stability of the film. The gas-sensing tests showed that ZnO hexagonal nanoplates exhibited sensitivity that was twice as high towards ethanol than ZnO nanorods at a similar optimum operating temperature of 300 °C. This difference was attributed to the larger surface area of the nanoplates compared to the nanorods (14.4 m^2/g vs. 7.43 m^2/g) and to the exposed (0001) planes of the nanoplates. By DFT simulation, the authors demonstrated a stronger adsorption of ethanol molecules on the (0001) ZnO planes as an effect of both the stronger adsorption energy of ethanol on O^- species and stronger hybridization between the adsorbed O2p orbital and the HOMO, HOMO − 1 molecular orbitals.

More recently, Xu et al. [34] by facile hydrothermal routes, synthesized two porous ZnO nanosheets with different exposed facets. The synthesized nanosheets had similar specific surface areas of about 7.5 m^2/g, thickness about 100 nm, lateral size about 5 μm, and pore size of 10 nm; however, their dominating exposed crystal facets were (0001) and (10$\bar{1}$0), respectively (Figure 3a–d). For the sensing measurements, a paste made of ZnO powders mixed with terpineol was coated on a ceramic tube with Au electrodes, subsequently sintered at 500 °C. According to what was already observed in previous works, the best sensing performance was obtained for nanosheets with exposed (0001) facets (Figure 3e), as also demonstrated by DFT simulation. In addition, by photoluminescence (PL) analysis the authors proved the presence of a large amount of oxygen vacancy defects and unsaturated dangling bonds existing in the ZnO nanosheets with exposed (0001) crystal facets. These, favoring the adsorption of gas molecules onto the material surface, resulted in the improvement of the gas response to ethanol.

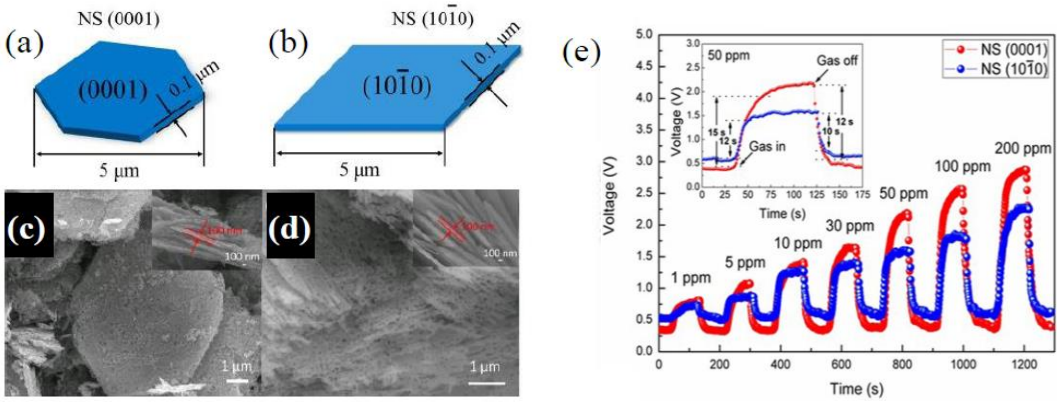

Figure 3. (**a**,**b**) Schematic representations of the crystal facets and (**c**,**d**) SEM images of ZnO nanosheets; (**e**) dynamic sensing characteristics of the sensors towards various ethanol concentrations, inset is the response/recovery curve of the sensors to 50 ppm ethanol at 330 °C. Reprinted from [34] with permission from Elsevier.

Xie et al. [47] fabricated a 3D porous hierarchical architecture through annealing of a zinc hydroxide carbonate precursor, which was obtained by a one-pot hydrothermal process with the assistance of carbon nanofibers and cetyltrimethyl ammonium bromide (CTAB). The ZnO hierarchical architectures were assembled from porous single crystal ZnO nanosheets with {0001} exposed crystal facets. The carbon nanofibers favored the formation of regular 3D hierarchical nanostructures and their stability after calcination. The gas sensor was fabricated coating a slurry of ZnO material onto an alumina tube with Au electrodes. Comparing the sensing properties of 3D hierarchical nanostructures with ZnO nanoclusters obtained in the absence of carbon nanofibers, a large improvement of sensing performances towards both ethanol and acetone were obtained. The enhanced gas-sensing properties of as-prepared porous ZnO hierarchical architectures were attributed to the unique structure, single crystal nature, and exposed polar crystal facets.

Zhang et al. [48] employed a hydrothermal method followed by annealing of the zinc carbonate hydroxide hydrate precursors at 300 °C in air, to synthesized porous 2D ZnO single crystal nanosheets with hexagonal wurtzite and mesoporous structures. A gas sensor based on these ZnO nanosheets, fabricated using an alumina tube with Au electrode, exhibited high response and fast response/recovery times in the range 0.01–1000 ppm of ethanol, a detection limit as low as 10 ppb (R_a/R_g = 3.05), and excellent selectivity and stability. The high ethanol response of the as-synthesized ZnO nanosheets was attributed to the large specific surface area due to single crystal porous structure, plane contact between nanosheets, 3D network architecture, and characteristically small thickness.

Liu et al. [49] reported the synthesis of a 2D ZnO structure made of single crystal flakes, which were grown on a silicon substrate using a combustion chemical vapor deposition (CVD) process with the assistance of methane flame. ZnO flakes, grown along <10$\bar{1}$0> directions, showed a cactus-like shape with thickness ranging from 150 to 250 nm. A gas sensor, fabricated by printing the ZnO flakes on patterned platinum electrodes, showed excellent sensitivity and fast response towards ethanol working at 400 °C. The authors attributed the excellent behavior only to the high surface to volume ratio of the structure.

Zhang et al. [50] prepared, on a large scale, ZnO hexagonal nanosheets by thermal annealing of simonkolleite ($Zn_5(OH)_8Cl_2 \cdot H_2O$) nanosheets synthesized via a one-pot hydrothermal method (Figure 4a,b). ZnO nanosheets were mixed with terpineol to form a slurry, which was coated on a ceramic tube and then annealed at 300 °C. they found that the annealing temperature dramatically affects the gas-sensing performance; in particular, the ZnO nanosheets annealed at 500 °C exhibited the best sensitivity to ethanol, with shorter response and recovery times (Figure 4c) than other samples. The enhanced gas-sensing performance was attributed to the optimal combination of porous structure, grain size, and the Cl element remaining in the structure of the material.

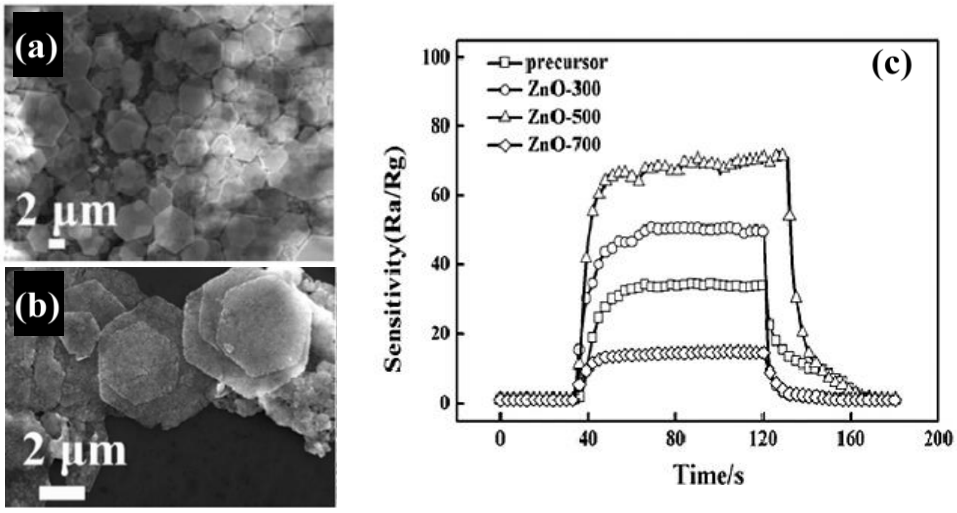

Figure 4. SEM image of simonkolleite precursor (**a**) and ZnO nanosheets after annealing at 500 °C (**b**), response/recovery curves to 100 ppm ethanol at 350 °C (**c**) Reprinted from [50] with permission from Elsevier.

Chen et al. [51] synthesized porous co-doped Sn–Rh ZnO nanosheets through a simple hydrothermal reaction process without any surfactant or template at 180 °C. A gas sensor was fabricated by coating the Au electrodes on a ceramic tube, with a paste of the ZnO product. The co-doped ZnO showed the best sensing performance for ethanol compared to pure and Sn doped ZnO nanosheets. The authors attributed the sensing performance of this material to the introduction of Sn ions in the ZnO structure, which leads to oxygen vacancy formation. In addition, due to the possible precipitation of rhodium oxide nanoparticles on the ZnO sheets, the formation of new Schottky barriers at the Rh_2O_3/ZnO interfaces could contribute to an enhancement in the sensing performance.

Fan et al. [52] prepared a 3D porous rod-like ZnO nanostructure by a simple precipitation method followed by calcination at 300 °C. These rod-like hierarchical structures were made by plenty of nanosheets with a thickness of 5–16 nm, interleaved with each other to form a net-like and wide open structure (Figure 5a). The ZnO powder mixed with ethanol was coated onto an alumina tube with a pair of Au electrodes and then aged at 200 °C. An excellent sensitivity to ethanol (Figure 5b) was reported, much higher than smooth 1D nanorods. The authors attributed the superior gas-sensing performance of the 3D hierarchical porous ZnO to its highly open, porous structure and the high specific surface area conferred by the interconnected 2D nanosheets.

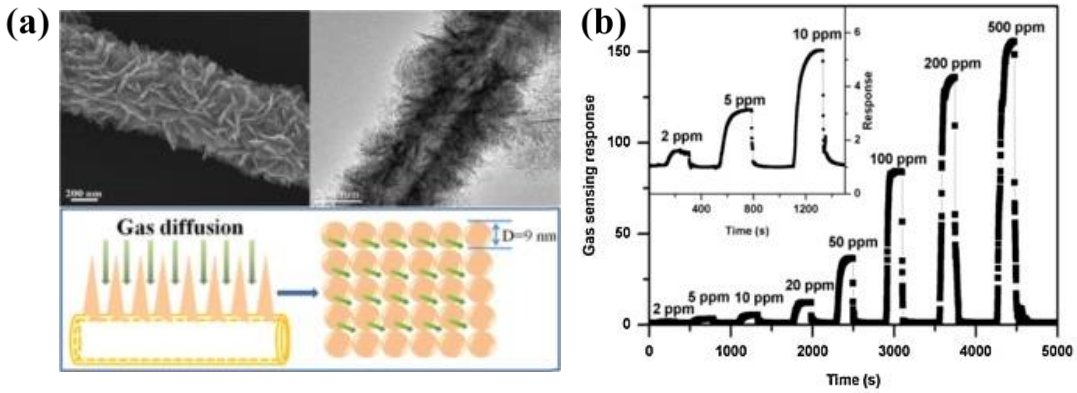

Figure 5. (**a**) SEM, TEM images, and schematic view of rod-like hierarchical structure; (**b**) dynamic responses to different concentrations of ethanol at 250 °C. Reprinted from [52] with permission from Elsevier.

Yu et al. [53] reported a facile preparation of 3D mesoporous ZnO film on planar Ag interdigitated electrodes substrate, which consisted of a uniform network of nanowalls ranging from 2 to 5 nm of thickness. Finally, the ethanol-sensing performance of the fabricated sensor was investigated. The authors considered that the contact resistance derived from the potential barriers at the nanowall junctions dominated the electrical properties of the material. Because the response of the gas sensor can be attributed to the apparent change of the potential barriers, more nanowalljunctions significantly increases the number of potential barriers, which results in an increased gas response.

Table 1 summarizes the gas-sensing properties of the above discussed 2D ZnO-based ethanol sensors.

Table 1. 2D ZnO-based ethanol sensors.

Material	Temperature (°C)	Concentration (ppm)	Response (R_a/R_g)	Response/Recovery Times (s)	Ref.
ZnO nanowhiskers	260	100	10.9	45/6	[29]
ZnO nanoplates	300	100	24.6	10/26	[11]
ZnO nanosheets	330	50	83.6	15/12	[34]
Hierarchical ZnO nanosheets	370	50	~145	12/30	[47]
ZnO nanosheets	400	200	398.43	7/19	[48]
ZnO flakes	400	300	8.8	62/62	[49]
ZnO nanosheets	340	100	70	14/19	[50]
Sn–Rh co-doped ZnO nanosheets	300	100	149.38	3/10	[51]
Tubular ZnO nanosheets	250	50	36.6	14/8	[52]
ZnO nanowalls	285	200	36.67	25/33	[53]

3.1.2. Acetone

Alenezi et al. [54], employing a facile hydrothermal route, developed three-dimensional hierarchical ZnO structures with a high surface-to-volume ratios and an increased fraction of (0001) polar surfaces. Starting from the synthesis of 1D single crystal nanowires and 2D nanodisks, followed by sequential nucleation and growth, elegant and extreme high surface to volume ratio hierarchical structures controlling the concentration of solution and the time of growth were prepared. In the first case, single nanowires with secondary rods (HZNWs) grown on them were obtained (Figure 6a,b). Similarly, starting from 2D nanodisks, secondary nanowires were grown along the [0001] direction on the top, bottom, and lateral sides of the nanodisks (HZNDs) (Figure 6c,d). ZnO nanostructures were deposited by spin coating on SiO_2/Si substrates with pre-patterned Au electrodes in order to fabricate the gas sensors. Both hierarchical ZnO structures displayed an enhancement of gas-sensing performance to acetone in comparison to the relative mono-morphological nanowires' and nanodisks' ZnO structures. In particular, HZNDs nanostructure showed the highest sensitivity, high saturation level, and shortest response and recovery times (Figure 6e,f). In addition to the high surface-to-volume ratio due to its small size, the authors ascribed the enhanced sensing properties to the increased proportion of exposed active (0001) planes that favors the chemisorption of oxygen species, and the formation of many nanojunctions at the interface between the initial ZnO nanostructure and secondary nanowires.

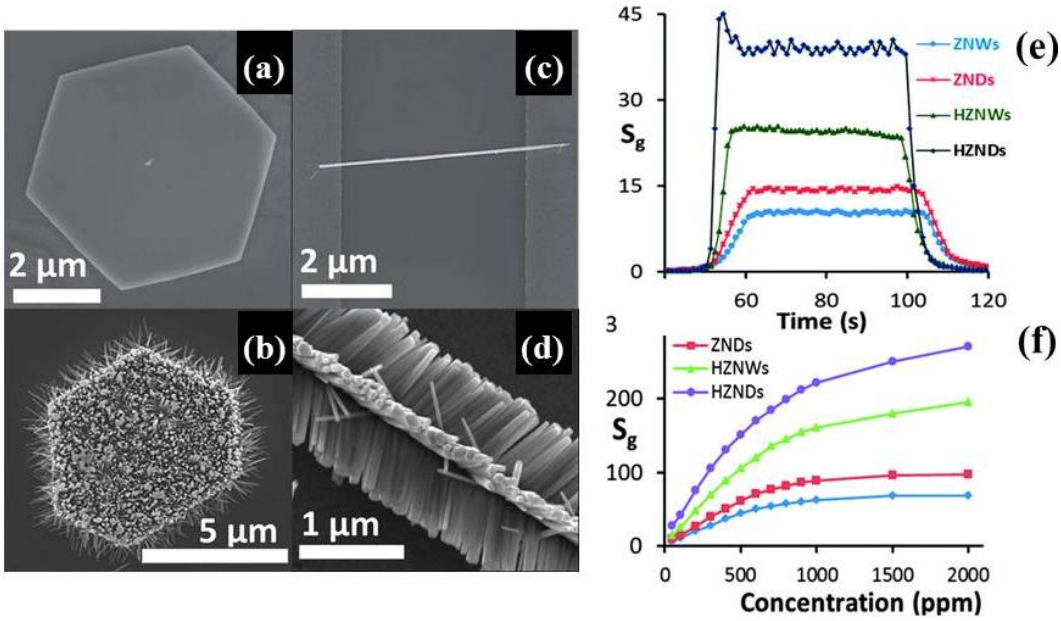

Figure 6. SEM images of singles (**a**) ZND; (**b**) HZND; (**c**) ZNW; and (**d**) HZNW; (**e**) dynamic responses to 100 ppm of acetone and (**f**) calibration curves of the four sensors at 350 °C. Reproduced from [54] with the permission of the Royal Society of Chemistry.

Xiao et al. [30] investigated the acetone sensing performance of pure and Pd nanoparticles decorated single-crystalline ZnO nanosheets with exposed (100) facets, synthesized by annealing of hydrozincite $Zn_5(CO_3)_2(OH)_6$ nanoplates produced with a water/ethylene glycol solvothermal method. Gas sensors were fabricated by printing a ZnO slurry on ceramic tubes with two Pt electrodes. The sensor made of Pd–ZnO nanosheets exhibited excellent sensitivity and selectivity to acetone. they suggested that the high percentage of exposed (100) facets may favor the selective adsorption of acetone molecules, while the Pd nanoparticles contributed to increase the sensitivity.

Al-Hadeethi et al. [55] synthesized 2D Sn-doped ZnO ultrathin nanosheets with sharp pointed edges and thickness about 20 nm (Figure 7a), by a simple hydrothermal method. A sensor, fabricated by printing a thick film of ZnO on alumina substrate decorated with Au electrodes, was tested towards acetone gas, which exhibited a maximum sensitivity of 5.556 (R_a/R_g) for 200 ppm of acetone at an optimal temperature of 320 °C (Figure 7b). The authors proposed that Sn doping resulted in distortions of lattice and O^- vacancy defects, which were the most susceptible adsorption sites for the generation of oxygenated anionic species from atmospheric molecular O_2.

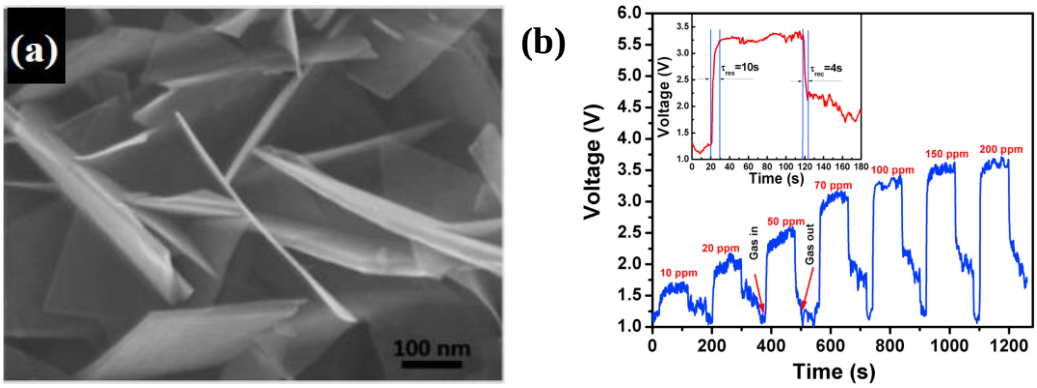

Figure 7. (**a**) SEM image of ZnO ultrathin nanosheets; (**b**) dynamic responses for 10–200 ppm of acetone at 320 °C. Reprinted from [55] with permission from Elsevier.

Fan and Jia [56], via a simple mixed hydrothermal synthesis in the presence of CTAB and 1,2-propanediol, synthesized 2D ZnO nanosheets with dimensions of several microns in length and 10–20 nm in thickness that are organized to form nanoflowers. A ZnO paste was coated on an alumina tube with a pair of Au electrodes used as the sensor. The gas-sensing tests showed the double ability to selectively detect acetone at a temperature of 360 °C and gasoline at 180 °C.

Wen et al. [57] developed a simple top-down route to prepare large porous ZnO flakes via template-free solution combustion synthesis followed by subsequent calcination in air. By this simple method, highly porous ZnO flakes, with tens to hundreds of micrometers in length and about 10 nm in thickness were obtained. The porous ZnO flakes were mixed with deionized water and then coated onto the outside of an alumina tube with two Au electrodes. The gas-sensing tests showed excellent sensitivity to both acetone and ethanol vapors as a result of the highly accessible 2D architecture, however, working at temperature as high as 485 °C. The highly porous structure shortens the diffusion distance and provides abundant transport channels and active surfaces for the target gas.

Behera and Chandra [58] presented a simple and cost-effective MEMS sensor incorporating ZnO–CuO nanoflakes. The material was synthesized by thermal oxidation in pure oxygen of a brass film deposited by radio frequency (RF) diode sputtering on silicon substrate. By this technique the authors obtained a homogenous film with flower-like structures consisting of sheets with a thickness of about 20–25 nm. The fabricated sensor was able to detect acetone, ammonia, and ethanol at a relatively low temperature (50 °C) although it showed an optimal response at 300 °C with improved selectivity to acetone.

Table 2 summarizes the gas-sensing properties of the above discussed 2D ZnO-based acetone sensors.

Table 2. 2D ZnO-based acetone sensors.

Material	Temperature (°C)	Concentration (ppm)	Response (R_a/R_g)	Response/Recovery Times (s)	Ref.
Hierarchical ZnO nanodisks–nanowires	425	100	44	2/4	[54]
Pd–ZnO nanosheets	340	100	70	9/6	[30]
Sn-doped ZnO nanosheets	320	100	3.9	10/4	[55]
ZnO nanosheets	360	50	31	2/15	[56]
ZnO flakes	485	100	22.2	-/-	[57]
ZnO–CuO nanoflakes	300	10	12.6	22/26	[58]

3.1.3. Formaldehyde

Guo [59] fabricated ZnO nanosheet–spheres with various Fe-doping concentrations by a one-step hydrothermal method. The synthesized materials were made of 3D nanospheres assembled by many single-crystal Fe–ZnO nanosheets. A paste of the sensitive materials was dropped onto alumina ceramic plate substrates to form a thick film between a pair of Ag–Pd interdigitated electrodes. The sensing properties towards 1–10 ppm formaldehyde were investigated for pure and Fe-doped ZnO nanosheets. The authors found the best performance at 300 °C for 2.5 wt% Fe doping with significantly enhanced sensitivity and selectivity, and short response and recovery times. The excellent performance was attributed to the large specific surface area of the 2.5 wt% Fe-doped sample that was damaged, increasing the dopant concentration. In addition, the key factor of Fe doping to enhance ZnO gas-sensing performance was attributed to structural and electronic sensitization such as narrowed bandgap, more electron donors, and oxygen vacancies (Vo), which were confirmed by UV-vis, PL, and XPS analysis.

Chen et al. [60] synthesized pure ZnO and graphene-modified ZnO using simple hydrothermal processes at 150 °C. Gas sensors were prepared by coating a paste of the materials onto an alumina tube with Au electrodes. Improving the regularity of pure ZnO nanosheets (ZnO-2), the sensitivity towards a low concentration of formaldehyde (10–500 ppm) was enhanced. In addition, by combining the best ZnO nanosheets with graphene, a large improvement of the sensing performance was obtained. In particular, loading ZnO with 2 wt% graphene (G-ZnO-2), the sensor exhibited excellent sensing

properties such as higher response, faster response/recovery times, as well as good selectivity at a lower temperature than pure ZnO nanosheets (200 °C) (Figure 8a,b). The improved gas-sensing properties of graphene-modified ZnO were mainly attributed to the larger work function of ZnO compared to graphene, which facilitates the migration of electrons from ZnO to the graphene sheets. Moreover, other benefits were attributed to the ability of ZnO nanosheets to adsorb oxygen species onto its surface and the narrower band gap, which gives rise to a higher carrier concentration than pure ZnO nanosheets at the same working temperature, thus facilitating the capture of oxygen.

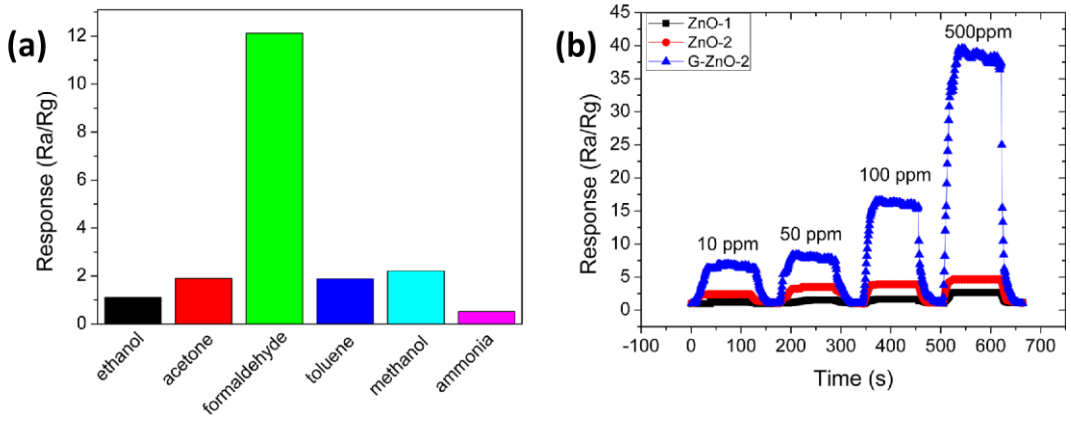

Figure 8. (**a**) Responses of the G-ZnO-2 sensor towards various gases (100 ppm) at 200 °C; (**b**) dynamic responses of two different pure (ZnO-1 and ZnO-2) and G-ZnO-2-based sensors in the concentration range of 10–500 ppm at 200 °C. Reproduced from [60] with permission of Springer.

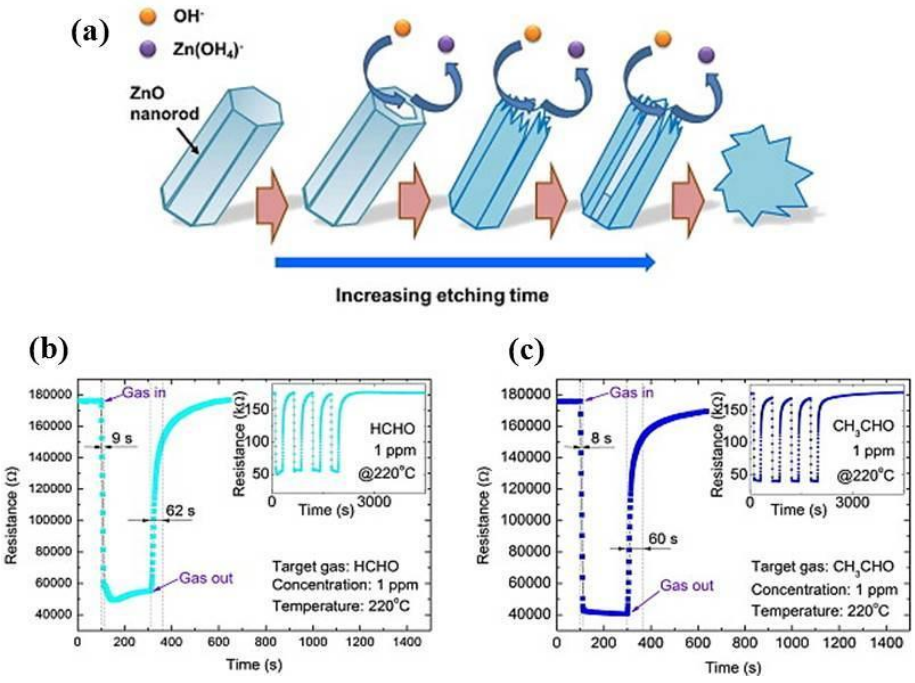

Figure 9. (**a**) Schematic illustration of the possible mechanism for ZnO nanosheet formation; dynamic responses of the ZnO nanosheets sensor to 1 ppm of (**b**) formaldehyde and (**c**) acetaldehyde. Reprinted from [61] with permission from Elsevier.

Zhang et al. [61] proposed a simple method for the large-scale production of dispersed single-crystalline ZnO nanosheets through a two-step process.

In the first step, ZnO nanorods were synthesized by a sonochemical method at room temperature using zinc nitrate hydrate without any surfactant, catalyst, or template. Then, ZnO nanosheets were fabricated by chemical etching of the ZnO nanorods in alkaline 1.5 M NaOH solution for 24 h (Figure 9a). The nanosheets had a size of 200–400 nm and thickness of about 10–60 nm. A microsensor substrate (1.8 mm × 1.8 mm with a 400 μm × 400 μm sensing area) was developed using MEMS technology where platinum electrodes and a micro-heater were deposited by sputtering with a patterned mask. Finally, a paste of ZnO nanosheet powder mixed with ethyl cellulose and terpineol was coated onto the MEMS substrate by a dropping method. Investigating the sensing performance, the authors showed a good ability of the ZnO nanosheets to detect the ppb-level of formaldehyde and acetaldehyde at the optimal operation temperature of 220 °C with a linear range from 50 ppb to 1 ppm and both response and recovery times lower than 1 min (Figure 9b,c).

Guo et al. [62] synthesized, by a simple hydrothermal method, ultrathin hexagonal ZnO nanosheets with a thickness of 17 nm and length of about 90 nm. they found that CTAB additive plays a critical role in producing such ultrathin ZnO nanosheets with exposed (0001) surfaces. A paste was next coated onto an alumina ceramic tube to realize a gas sensor. The sensing measurements revealed that the sensor made of these hexagonal ZnO nanosheets exhibited an excellent response to 50 ppm of formaldehyde with both response and recovery times close to 10 s at an optimal temperature of 350 °C.

Table 3 summarizes the gas-sensing properties of the above-discussed 2D ZnO-based formaldehyde sensors.

Table 3. 2D ZnO-based formaldehyde sensors.

Material	Temperature (°C)	Concentration (ppm)	Response (R_a/R_g)	Response/Recovery Times (s)	Ref.
Fe-doped ZnO nanosheet–spheres	300	10	33.1	42/11	[59]
ZnO nanosheets graphene	200	100	12.5	10/29	[60]
ZnO nanosheets	220	1	~3.2	9/62	[61]
ZnO nanosheets	350	50	37.8	9/11	[62]

3.1.4. n-Butanol

Kaneti et al. [28] presented a simple one-step hydrothermal approach under mild conditions (150–180 °C) and without high-temperature calcination, for the synthesis of ZnO nanoflakes with exposed $(10\bar{1}0)$ surfaces. The ZnO nanoflakes mixed with PVDF were coated on a ceramic tube with printed Au electrodes. A treatment at 450 °C was adopted to remove the binder. The gas-sensing properties of the as-synthesized ZnO nanoflakes were excellent and they also demonstrated good stability towards different VOCs—with the highest sensitivity and selectivity to n-butanol—at the optimal working temperature of 330 °C. The authors showed that the sensing mechanism was related to surface reactions with O^{2-}, also confirming that at temperatures above 300 °C, these are the predominant oxygen species absorbed onto the surface of the ZnO. In addition, employing a molecular dynamics (MD) simulation, the diffusion and adsorption of different VOCs onto $(10\bar{1}0)$ $(11\bar{2}0)$ and (0001) surfaces of ZnO at 330 °C were investigated. they found that the lowest diffusivity was shown by n-butanol on the $(10\bar{1}0)$ facet due to the heavier molecular weight, lower than other ZnO surfaces. This result may explain the higher sensitivity to n-butanol of the prepared ZnO nanoflakes in comparison to other alcohol molecules with smaller molecular weight.

Chen et al. [63] prepared by a two-step hydrothermal method a p–n junction ZnO–CuO nanostructure. In the first step, 2D porous ZnO nanosheets with exposed (0001) facets were assembled to form spheres. During the second hydrothermal process, leaf-like 2D CuO structures were grown outward on the surface of ZnO nanosheets (Figure 10a–c). A proper amount of ZnO or CuO–ZnO composite powders were mixed with distilled water to form a paste, which was then coated onto an alumina tube with a pair of Au electrodes. Comparing the sensing performance towards different VOCs, an increased sensitivity of ZnO–CuO nanostructures was found in comparison to pure ZnO.

In particular, the sensitivity to n-butanol of the nanocomposite was 2.7-fold higher than pure ZnO at 220 °C, with excellent selectivity (Figure 10d). The authors attributed the enhanced sensitivity to the electronic sensitization due to the p–n junction. In addition, the porous and open 2D/2D heterostructure, favoring the fast diffusion and easy adsorption of gas molecules, contributed to the superior sensing performance of the composite.

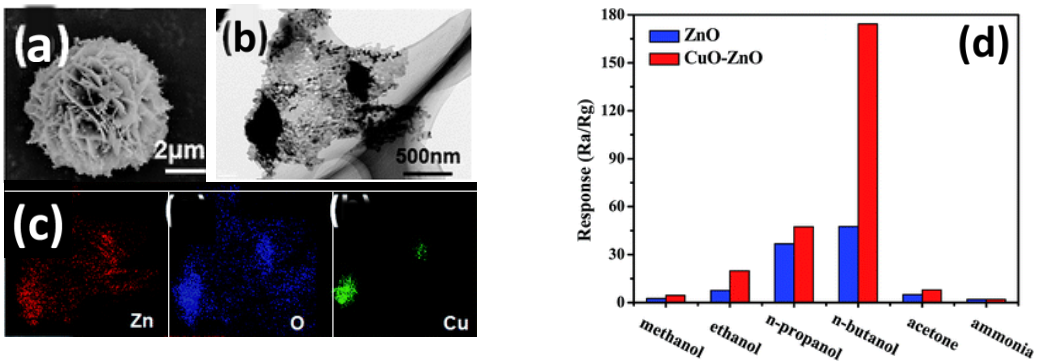

Figure 10. (**a**) SEM image, (**b**) TEM image, and (**c**) corresponding elemental mapping of the CuO–ZnO composite, (**d**) response of ZnO and CuO–ZnO composite sensors to various 100 ppm VOC gases at 200 °C and 220 °C, respectively. Reproduced from [63] with the permission of the Royal Society of Chemistry.

Wang et al. [64], by a hydrothermal method, prepared ZnO microsheets with exposed (0002) crystal planes functionalized with Au nanoparticles. A paste was coated onto an alumina tube with a pair of Au electrodes to realize the gas sensors. The sensing tests showed that the Au NPs-functionalized porous ZnO microsheets sensor exhibited enhanced performance towards several VOCs including, ethanol, methanol, acetone, benzene, and, markedly to n-butanol. The enhanced sensing properties were related to the unique structure of porous ZnO microsheets and the strong spillover effect of small Au nanoparticles that catalyze the sensing reactions, as well as the increase of Schottky barriers caused by the electronic interaction between Au and ZnO.

Huang et al. [65], by a very simple solution method at near room temperature, prepared a flower-like ZnO nanostructure self-assembled by thin and uniform 2D nanosheets with a thickness of approximately 18 nm. The as-prepared flowerlike ZnO nanostructures were directly coated onto the outer surface of an alumina tube with a pair of Au electrodes. The gas-sensing measurements showed that the flowerlike ZnO nanostructures exhibited high sensitivity, fast response/recovery, and good reversibility towards some reducing gases, with the best sensitivity to both n-butanol and ethanol at a working temperature of 320 °C. The authors simply attributed the good sensing performance to the small thickness of ZnO nanosheets and 3D structures of the flowerlike ZnO nanostructures.

Table 4 summarizes the gas-sensing properties of the above-discussed 2D ZnO-based n-butanol sensors.

Table 4. 2D ZnO-based n-butanol sensors.

Material	Temperature (°C)	Concentration (ppm)	Response (R_a/R_g)	Ref.
ZnO nanoflakes	330	100	54.4	[28]
CuO–ZnO nanosheet–spheres	220	20	37.7	[63]
Au–ZnO microsheets	240	20	18.5	[64]
Flower-like ZnO nanosheets	320	100	24.1	[65]

3.1.5. Other VOCs

Gu et al. [66], via a one-pot hydrothermal method followed by a liquid phase reduction process, synthesized Pt-decorated porous single-crystalline ZnO nanosheets. Adjusting the amount of reduction

agent ($NaBH_4$), a homogenous dispersion of Pt nanoparticles was obtained that improved the sensing performance of the synthesized Pt-decorated ZnO nanosheets. The sensing materials were dispersed in ethanol and then coated onto the ceramic tube to fabricate a sensor. The authors showed that Pt decoration leads to a better sensing performance to chlorobenzene than either Au- or Ag-decorated ZnO nanosheets. In particular, the Pt–ZnO nanosheets showed fast response/recovery times, and high sensitivity and selectivity to ppb levels of chlorobenzene vapor in comparison to other VOCs at 300 °C. The excellent sensing performance was attributed to the electronic and chemical sensitization effects of Pt nanoparticles.

Jing and Zhan [67], by simple microwave synthesis followed by annealing at 400 °C, synthesized ZnO nanoplates with an edge thickness lower than 19 nm. The synthesized ZnO nanoplates were mixed with water and then coated onto an alumina tube. Investigating the sensing performance of the synthesized ZnO nanoplates, the authors observed excellent sensitivity to chlorobenzene in the range 100–250 ppm at an optimal temperature of 200 °C. In addition, the same material showed excellent sensitivity in the same range of concentration to ethanol but at higher temperature.

Zhang et al. [68] synthesized ZnO architectures composed of nanorods and nanosheets-assembled microspheres through a one-pot hydrothermal process at low temperature. The ZnO products were ground with Triton X-100 and then the paste was coated on an alumina tube with Au electrodes. The gas-sensing property of the ZnO architectures displayed high response, fast response/recovery times, good selectivity, and long-term stability to 1–1000 ppm dimethylamine at 370 °C (Figure 11a).

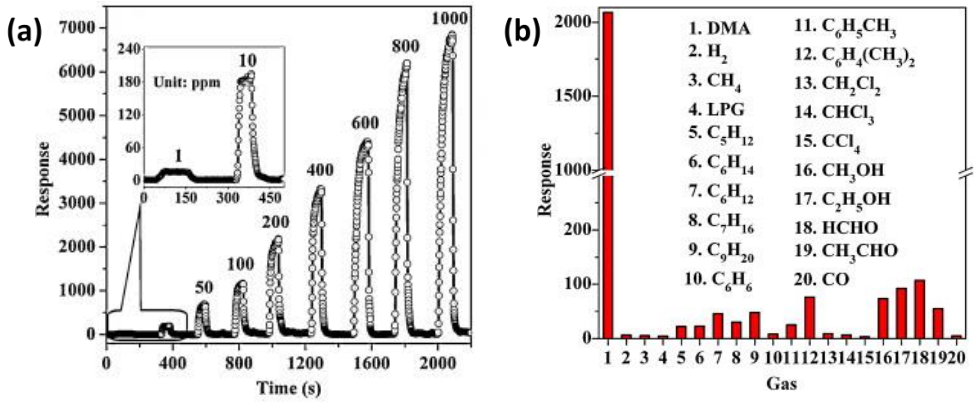

Figure 11. (**a**) Dynamic responses of the sensor to dimethylamine in the range of 1–1000 ppm at 370 °C; (**b**) selectivity of the sensor to 200 ppm dimethylamine and other 19 interfering gases. Reprinted from [68] with permission from Elsevier.

In particular, the synthesized ZnO architecture showed better selectivity to this analyte than many other VOCs and homologous compounds such as trimethylamine, methylamine, and ammonia (Figure 11b). By photoluminescence and XPS analysis, the authors observed a large amount of chemisorbed oxygen species induced by a high content of electron-donor defects, to which was attributed the high response to dimethylamine.

Tonezzer et al. [69] grew directly, on a silicon substrate, 1D ZnO nanowires and 2D ZnO nanosheets, then investigated their sensing performance towards liquid petroleum gas (LPG). Under the same operating conditions, the ZnO nanowires showed a better response when compared to ZnO nanosheets of similar thickness, although the latter nanostructure demonstrated an improved limit of detection (LoD). Although the authors attributed the improved sensitivity of the nanowires to the higher surface to volume ratio, they explained the lower LoD by the more stable base current shown by this nanostructure. However, there was no discussion of the exposed crystal faces.

Kaneti et al. [70], by a hydrothermal method, synthesized ZnO nanoflakes with exposed $(10\bar{1}0)$ facets and high porous surface with diameters ranging from 2 to 20 nm. The ZnO nanoflakes were also decorated with Au nanoparticles using three different loads of 1.37, 2.87, and 5.41 wt%, respectively.

ZnO samples were mixed with PVDF and 1-methyl-2-pyrrolidone to form a white slurry, which was then coated on ceramic tubes with Au electrodes. A treatment at 350 °C was used to remove the polymeric binder. Testing the gas-sensing behavior towards n-butylamine, the authors found that, compared to pure ZnO nanoflakes, 2.87 wt% Au-decorated samples exhibited greatly enhanced selectivity, a decrease in optimal operating temperature from 300 to 240 °C, about 6-fold higher response and up to 2.5-fold faster response and recovery times. By DFT simulation the interaction between the nitrogen atom of n-butylamine and $(10\bar{1}0)$ ZnO surfaces was demonstrated to favor the adsorption of this species over other VOCs. In addition, Au decoration increased the quantity of adsorbed oxygen species onto the ZnO surface, leading to the formation of a depletion layer at the ZnO/Au interface. This resulted in a significantly improved response of the ZnO/Au sensors towards n-butylamine.

Table 5 summarizes the gas-sensing properties of the above-discussed 2D ZnO-based VOCs sensors.

Table 5. 2D ZnO-based VOCs sensors.

Material	VOC	Temperature (°C)	Concentration (ppm)	Response (R_a/R_g)	Response/Recovery Times (s)	Ref.
Pt–ZnO nanosheets	Chlorobenzene	300	0.03	6.1	20/10	[66]
ZnO nanoplates	Chlorobenzene	200	100	6.9	103/22	[67]
ZnO nanosheets–nanorods microspheres	Dimethylamine	370	200	2086.9	16/15	[68]
ZnO nanosheets	LPG	250	500	1.5	15/29	[69]
Au–ZnO nanoflakes	n-butylamine	240	50	73.2	~25/25	[70]

3.2. Nitrogen Dioxide

Nitrogen dioxide (NO_2) is a pungent red-brown oxidizing gas considered one of the main air pollutants, with serious adverse effects on health and environment. It is mainly produced by fossil fuel combustion at high temperature and, in particular, by internal combustion engines. Different ZnO nanostructures have been synthesized, investigated, and effectively employed as NO_2 gas sensors. A deep analysis of these works showed that the sensing properties of ZnO towards NO_2 were strongly influenced by morphology and particle sizes, as well as by the exposed crystallographic planes of the nanostructure [35]. Driven by the latter aspect, many papers have been devoted to the synthesis of 2D materials, where specific facets are exposed, then investigated for their sensing properties towards NO_2.

Yu et al. [71] grew well-aligned ZnO nanowalls on an ITO glass substrate via a two-step aqueous solution, using zinc acetate and aluminum nitrate as the source materials. The authors showed that Al^{3+} played a critical role in synthesis because it supported nucleation for ZnO nanowalls. Then, the sensing properties towards NO_2 in the concentration range of 1–50 ppm at high temperature were investigated. In a subsequent work [72], the effect of annealing temperature ranging from 350 °C to 750 °C on ZnO nanowalls' morphology and gas-sensing properties were also investigated. The as-prepared ZnO nanowalls exhibited a triangular pore structure composed of cross-link walls with 20 nm thicknesses grown preferentially along the [001] direction (Figure 12a). The samples maintained the morphology up to 450 °C while, at higher temperatures, it was degraded with the disappearance of some porosity, which, in turn, decreased the effective surface area. The authors, investigating the sensing properties towards 50 ppm NO_2 at room temperature, obtained the best sensing response with fast response and recovery times (23 and 11 s) and good repeatability for the sample annealed at 450 °C (Figure 12b). A combination of oxygen vacancies defects due to annealing treatments, and porosity due to the interconnected nanostructure, was suggested as the motivation of the sensing performance.

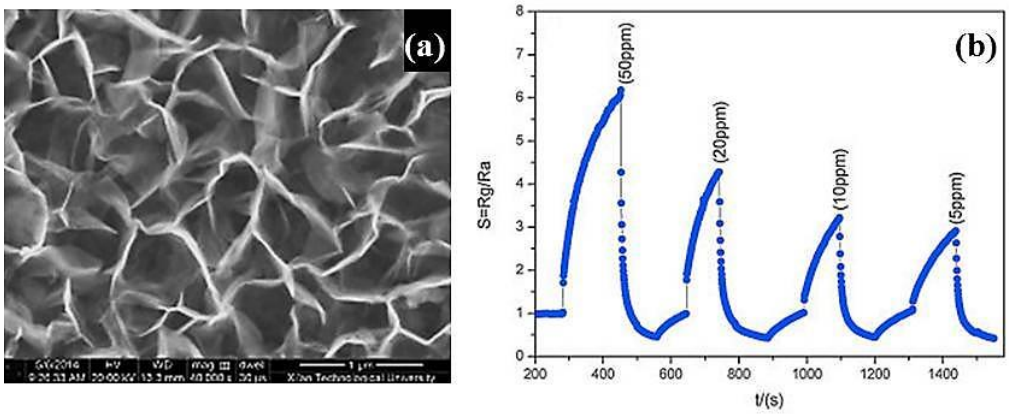

Figure 12. (**a**) SEM image of ZnO nanowalls annealed at 450 °C; (**b**) dynamic responses under exposure to NO_2 gas with different concentrations ranging from 5 to 50 ppm at room temperature. Reprinted from [72] with permission from Elsevier.

A similar investigation was carried out by Chen et al. [73] using polygonal ZnO nanoflakes synthesized by a microwave hydrothermal method. The as-prepared zinc nitrate hydroxide nanoflakes precursors were annealed at different temperatures ranging from 300 °C to 600 °C, in order to obtain porous ZnO nanoflakes with a thickness of 40–80 nm, consisting of no more than two layers of irregular ZnO primary nanoparticles. The ZnO was mixed with water to form a slurry, then spread onto an alumina tube with a pair of Au electrodes and finally aged at 300 °C. The authors investigated the gas-sensing performance towards 0.5 ppm NO_2 and found 500 °C to be the best annealing temperature with the highest response. Analyzing the behavior of sensor response with the increased particle sizes as an effect of annealing temperature, they found no correlation. Rather, by PL and XPS measurements, it was proven that the intensities of donors (oxygen vacancy and/or zinc interstitial) and surface oxygen species were involved in the sensing mechanism, leading to the different gas-sensing properties of each annealed sample. In addition, the 500 °C-annealed ZnO nanoflakes showed excellent sensitivity with a linear response in the range 0.05 ppm to 10 ppm NO_2 and good selectivity to other gases.

Wang et al. [74] synthesized hierarchical nanosheet–nanorods architectures (NS–NR) for compositing with poly(3-hexylthiophene) (P3HT) by a one-step solution method. A silicon wafer was used as the sensor substrate where Ti–Au interdigitated electrodes were deposited by RF sputtering. Finally, an ethanol/water suspension of the material was spin-coated onto the electrodes. The P3HT/ZnO NS-NR bilayer film exhibited not only the highest sensitivity but also good reproducibility and selectivity to NO_2 at room temperature. The enhanced sensing performance was attributed to the formation of P3HT/ZnO heterojunction as well as the high content of oxygen vacancy defects on the surface of NS-NR architectures.

Xiao et al. [19] synthesized ZnO nanosheets by a facile ultrathin liquid layer electrodeposition method on a silicon substrate. ZnO nanosheets with an average thickness of 20 nm and (100) exposed facets, were interwoven to form an extensive porous network. Au electrodes were deposited on the ZnO nanosheets by vacuum ion sputtering in order to connect to the electrical circuit. The authors, investigating the sensing performance towards NO_2 in the range 1–400 ppm, found the optimal operating temperature at 180 °C. At this condition, a ZnO nanosheet-based sensor showed high response, fast response/recovery times (3 s and 12 s to 10 ppm NO_2, respectively), and excellent selectivity. The abundant oxygen vacancies on the (100) exposed surfaces were considered the active sites for NO_2 adsorption, which were responsible of the high response observed.

Chang et al. [27], by a hydrothermal method, synthesized 3D ZnO nanostructures made of self-assembled 20 nm thick nanosheets with exposed {0001} crystal facets. By properly monitoring the molar ratio of the zinc precursor and urea, flower-like (Figure 13a) and grass-like (Figure 13b) ZnO porous structures were obtained. The authors prepared gas sensors by spin coating deposition of both

ZnO nanostructures onto Au interdigitated electrodes on SiO_2 substrates. The gas-sensing properties towards 0.5–10 ppm NO_2 were compared with a sensor made of commercial ZnO nanoparticles. Both flower-like (ZnO-F3) and grass-like (ZnO-F5) nanostructures showed higher response compared to ZnO nanoparticles, with ZnO-F3 exhibiting much higher sensitivity to NO_2 gas at an optimal operating temperature of 200 °C. The superior gas-sensing performance of flower-like ZnO was attributed to the higher oxygen vacancies and the morphology maintained after sensor preparation, which provides a higher surface for the gas adsorption.

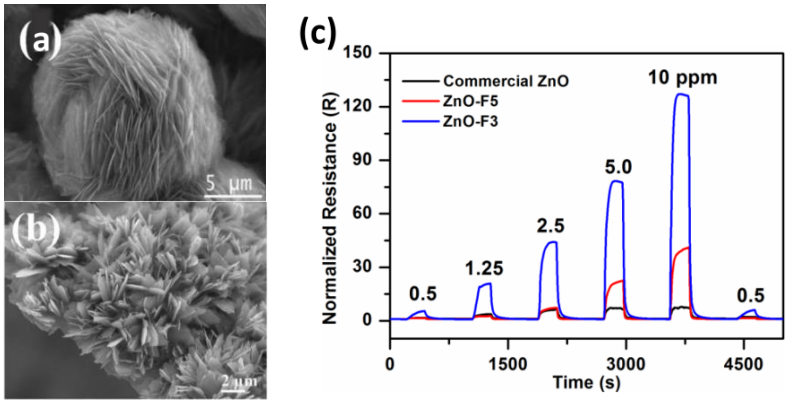

Figure 13. SEM images of ZnO samples (**a**) F3 and (**b**) F5; (**c**) dynamic response curves of the sensors prepared from F3, F5, and commercial ZnO samples to NO_2 with concentrations ranging from 0.5 ppm to 10 ppm at 200 °C. Reproduced from [27].

Mun et al. [75] synthesized Au-decorated ZnO nanosheets using a three-step process consisting of ZnO fabrication by a thermal evaporation of Zn powder, Au sputter deposition, and thermal annealing at 700 °C. For the fabrication of the sensor, Ni and Au thin films were deposited by sputtering to form interdigitated electrodes on a silicon substrate, then ZnO nanosheets suspended in ethanol were poured on the electrodes. The sensing performances towards 1–5 ppm NO_2 at room temperature, and under 365 nm UV irradiation, were investigated. The response to NO_2 was strongly improved, increasing the intensity of UV illumination from dark to 1.2 $mW \cdot cm^{-2}$ (Figure 14a). In addition, Au functionalization improved up to 3.3-fold compared to pure ZnO nanosheets (Figure 14b). The sensor also showed a fast response time of about 6 s to 5 ppm NO_2. The significant enhancement in the response of the ZnO nanosheets to NO_2 gas by UV irradiation was attributed to the increased change in resistance due to the photogeneration of electrons and holes.

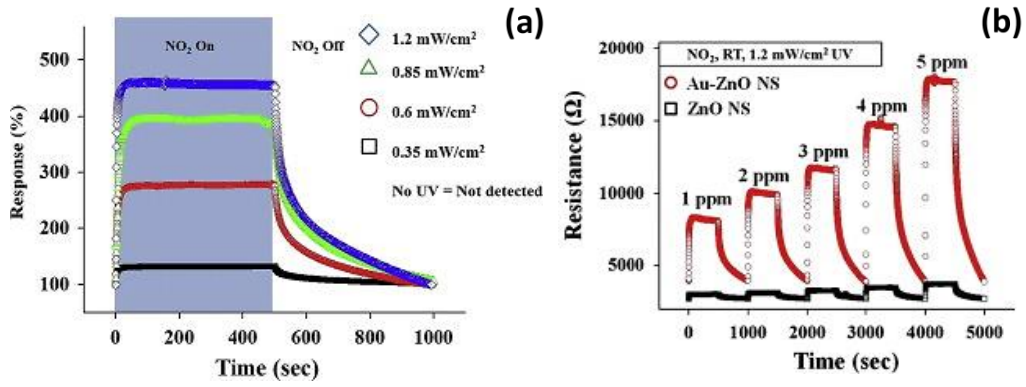

Figure 14. (**a**) Dynamic responses of Au–ZnO nanosheets to 5 ppm NO_2 for different UV light illumination intensities; (**b**) dynamic responses of Au-ZnO nanosheets to 1–5 ppm NO_2 at room temperature under UV light illumination. Reprinted from [75] with permission from Elsevier.

Table 6 summarizes the gas-sensing properties of the above-discussed 2D ZnO-based NO_2 sensors.

Table 6. 2D ZnO-based NO_2 sensors.

Material	Temperature (°C)	Concentration (ppm)	Response (R_g/R_a)	Response/Recovery Times (s)	Ref.
ZnO nanowalls	220	50	30	30/48	[71]
ZnO nanowalls	RT	50	6.4	22/11	[72]
ZnO nanoflakes	180	1	~135	-/-	[73]
P3HT/ZnO nanosheet–nanorods	RT	4	1.6	-/-	[74]
ZnO nanosheets	180	10	3.58	3/12	[19]
Flower-like ZnO nanosheets	200	5	~75	~60/60	[27]
Au–ZnO nanosheets	RT/365 nm UV irradiation	5	~5.5	6/320	[75]

3.3. Carbon Monoxide

Carbon monoxide (CO) is an odorless, colorless pollutant gas produced by the incomplete combustion of fuels and is commonly found in automotive exhaust gas. Together with nitrogen dioxide, CO is considered one of the most dangerous pollutant gases. Prolonged exposure to concentrations higher than 50–70 ppm of CO may cause death [13]. Many different nanostructures based on pure and doped ZnO have been investigated as sensitive materials for CO monitoring [13,76–78]. Despite this, only a few studies have reported the use of 2D ZnO as a CO sensor.

Jones and Maffeïs [79] used ZnO nanosheets to create a mathematical model of the surface reactions of CO on this material. The ZnO nanosheets were produced by thermal decomposition at 500 °C of layered basic zinc acetate, synthesized by a microwave method. The sheets, with a thickness of 20–100 nm, consisted of multiple nanoparticles with an average diameter of 38 nm (Figure 15a). The authors experimentally investigated the response to different CO concentrations ranging from 50 ppm to 200 ppm at different operating temperatures from 393 °C to 484 °C. Then, under the assumption that the CO reacts only with surface oxygen species via an Eley–Rideal mechanism, they demonstrated that the measured resistance responses of the system are well described by the theoretical model presented (Figure 15b).

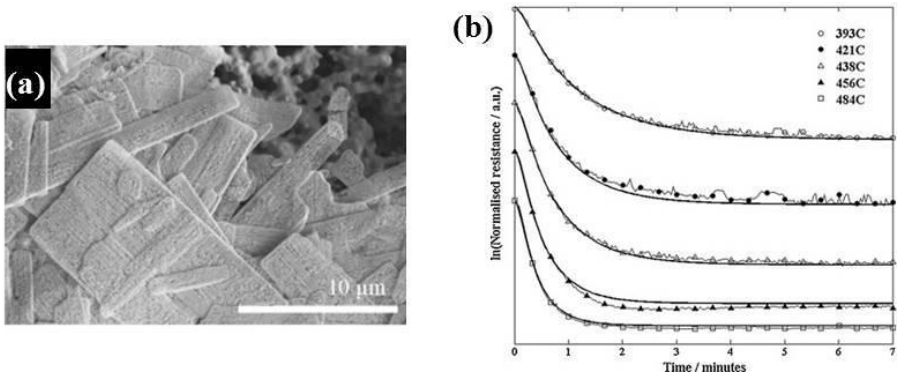

Figure 15. (**a**) SEM image of ZnO nanosheets; (**b**) dynamic response curves at different working temperatures to a CO concentration of 200 ppm (dots) and fitted by mathematical model (bold lines). Reprinted from [79] with permission from Elsevier.

Zeng et al. [80] prepared a sensor based on hierarchically porous ZnO nanosheet thin films vertically grown on a silicon substrate, using a facile two-step solution phase method. In the first step, a ZnO layer was preferentially deposited by the sol-gel method on the substrate. In the second step, ZnO nanosheets with a thickness of about 30 nm were subsequently grown by a facile solvothermal process. The Si-based sensor was achieved using a conventional photolithography process where Pt interdigital electrodes and heater were sputtered on a silicon substrate. Then, the gas-sensing performance of the as-prepared sensor towards CO in the range of 5 ppm to 500 ppm was investigated.

they found excellent sensitivity (R_a/R_g = 11.2 at 100 ppm CO) and short response/recovery times (25 s and 36 s, respectively) at an optimal temperature of 300 °C with good selectivity against typical interfering gases such as SO_2, NO_2, NH_3, H_2, and VOCs. The less agglomerated and porous network of the structure, in addition to providing a high surface area, favors rapid access to the surface and effective diffusion of CO molecules.

Chang et al. [81], starting from zinc powder, grew ZnO nanowalls on a glass substrate through a catalyst-free process in a tube furnace. By this simple method, they obtained interconnected ZnO nanowalls with (0001) exposed crystal planes, vertically grown from a glass substrate, with width and height typically ranging from 70 nm to 200 nm and 3.7 nm to 6.5 μm, respectively. Investigating the gas-sensing performance towards CO in the range 100 to 5000 ppm, the highest sensitivity was found at 300 °C with a response $(I_g - I_a)/I_a$ = 0.3 to 100 ppm CO.

3.4. Ammonia

Ammonia (NH_3) is generally produced by natural processes in animals, humans, and plants, and is a widely used chemical. However, it is acutely toxic if inhaled above a moderate quantity as low as 25–35 ppm [82]. Numerous studies have been focused to the use of pure and doped ZnO thin films as NH_3 sensitive materials [83–85].

As regards 2D ZnO nanostructures, Liu et al. [86] fabricated single-crystalline ZnO nanosheets with a highly porous structure by annealing a $ZnS(en)_{0.5}$ (en = ethylenediamine) complex precursor synthesized by a solvothermal route. The $ZnS(en)_{0.5}$ precursor exhibited a rectangular shape with [0001] growth direction with a size of about 800 nm × 500 nm and a thickness of approximately 15 nm. After a thermal treatment at 600 °C in air, the same shape of precursor was maintained but numerous pores with a size distribution from 20 to 30 nm were formed on the nanosheets (Figure 16e,f). The authors also proposed that the substitution of S by O atoms, rather than the decomposition of organic components in the complex precursor, is the explanation for the formation of the porous structure. A gas sensor was fabricated by coating an ethanol suspension of the ZnO nanosheets onto the surface of an alumina planar substrate with comb-like gold electrodes. The gas sensor based on the synthesized porous ZnO nanosheets showed excellent performance in detecting NH_3 in the range from 50 ppm to 500 ppm, and similar performance towards formaldehyde. In particular, at 250 °C the sensor showed response and recovery times ranging from 3 s to 15 s and from 6 to 24 s, respectively (Figure 16a–d). they suggested that the mesoporous structure allows for fast diffusion of gas molecules, resulting in high rates of gas adsorption and desorption.

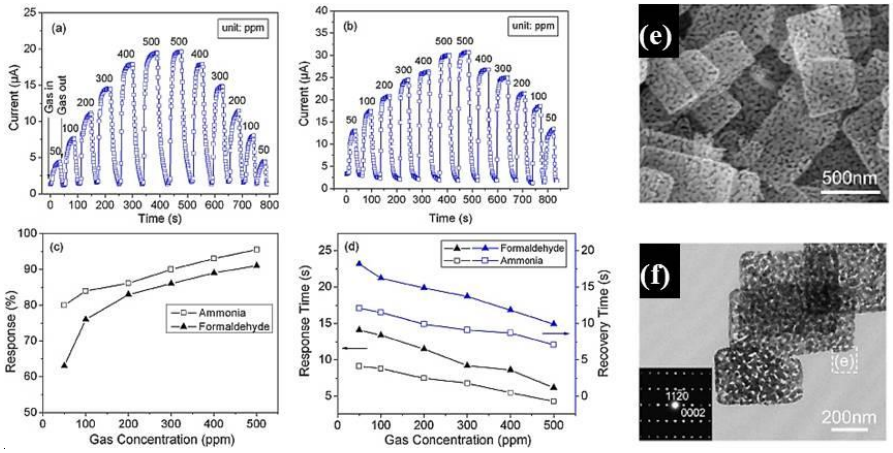

Figure 16. Gas-sensing performance of the gas sensor based on the porous single crystalline ZnO nanosheets: the dynamic responses towards (**a**) formaldehyde and (**b**) ammonia; (**c**) calculated responses, and (**d**) response/recovery times at 250 °C; (**e**) SEM and (**f**) TEM images of ZnO nanosheets after annealing at 600 °C. Reproduced from [86] with the permission of IOP Publishing.

Nguyen et al. [87], by a hydrothermal method, synthesized ZnO nanoplates made of single-crystal wurtzite structure with a thickness of 40 nm and 200 nm × 400 nm in lateral dimensions. The authors also prepared composites by mixing the synthesized ZnO nanoplates and WO_3 nanorods with different weight ratio. A gas sensor was fabricated by drop-coating of a ZnO slurry onto a Pt-interdigitated electrodes, then annealing it at 400 °C in air.

Investigating the sensing performance to NH_3, increased sensitivity and a decrease in the optimal operation temperature from 300 °C to 250 °C, for the 1:1 WO_3/ZnO composite, were observed in comparison to the pure phases. In addition, a low response to ethanol, acetone, and LPG suggested a good selectivity to NH_3. The authors hypothesized that the sensing properties of WO_3/ZnO composites were determined not only by their specific surface area but also by electronic sensitization of the heterojunction.

Li et al. [88] presented a new way to obtain ZnO nanosheets grown in situ on a ceramic substrate equipped with Au electrodes, via a hydrothermal treatment of electrospun nanofibers from polyvinyl alcohol and zinc acetate. By acting on the temperature and duration of hydrothermal treatment, nanoparticles or nanosheets were obtained. Due to the high resistance at room temperature of sensors based on synthesized materials, the ZnO nanostructures were covered with a thin layer of polypyrrole (PPy). The obtained PPy/ZnO nanohybrids showed a reduction in electrical resistance and a relatively fast and high response to concentrations ranging from 0.5 to 10 ppm of NH_3 at room temperature. In particular, comparing the sensing performance of PPy/ZnO nanoparticles with PPy/ZnO nanosheets, the latter presented markedly enhanced sensitivity and low saturation. Moreover, a good selectivity to NH_3 was observed in comparison to a number of gases, including common volatile organic solvents and several organic amines. The authors used the reduction in electrical resistance and the superior sensing properties to explain the establishment of a p–n junction between PPy and ZnO.

Table 7 summarizes the gas-sensing properties of the above-discussed 2D ZnO-based NH_3 sensors.

Table 7. 2D ZnO-based NH_3 sensors.

Material	Temperature (°C)	Concentration (ppm)	Response (R_a/R_g)	Response/Recovery Times (s)	Ref.
ZnO nanosheets	250	50	2.63	8/14	[86]
WO_3–ZnO nanoplates	250	300	24	60/50	[87]
PPy/ZnO nanosheets	RT	5	1.55 [1]	256/370	[88]

[1] Response R_g/R_a.

3.5. Other Gases

Fu et al. [89] developed a facile method to fabricate a porous 2D net-like SnO_2/ZnO heteronanostructure using graphene sheets as a hard template. In the first step, a graphene/SnO_2/ZnO composite was obtained by a wet chemical method. In the second step, the as-synthesized sample was treated at 500 °C in air in order to decompose the carbon matrix and obtain a 2D porous net-like SnO_2/ZnO heteronanostructure (Figure 17a–c). For the fabrication of the gas sensor, the sample was dissolved in ethanol and a drop was spun on a ceramic tube between metal electrodes to form a film with a thickness of about 0.1 mm. The authors investigated the sensing performance of the synthesized nanostructure towards hydrogen sulfide (H_2S) at various working temperatures. they obtained a very high response to 5 ppm H_2S at an optimal temperature of 100 °C with a resistance ratio (R_a/R_g) of 112, which was about 3.5 and 10 times higher than the SnO_2 and ZnO pure phases, respectively (Figure 17d,e). The improved response shown by the SnO_2/ZnO nanostructure was attributed to the small size of the particles in the heteronanostructure compared to the pure phases, and the formation of heterojunctions at the interfaces. In addition, the better selectivity compared to other species was attributed to the ability of H_2S to form a metal sulfide on the surface of metal oxides, which leads to a large variation in the resistance.

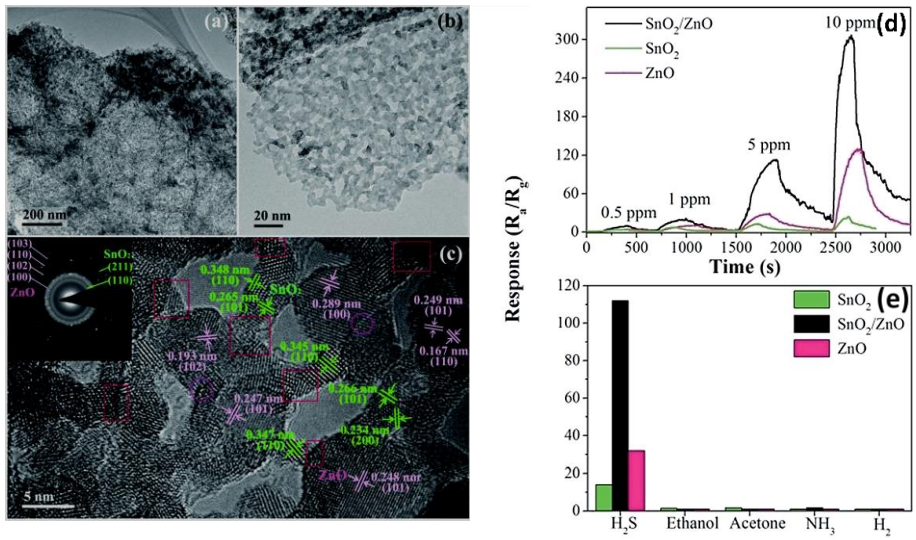

Figure 17. (**a**) Low-magnification TEM, (**b**) high-magnification TEM, and (**c**) HRTEM images of SnO_2/ZnO heteronanostructure; (**d**) dynamic responses of the sensors based on nanostructures at 100 °C and (**e**) selectivity with 5 ppm H_2S and 100 ppm for the other gases. Reproduced from [89] with the permission of the Royal Society of Chemistry.

Chen et al., in two different papers [90,91], investigated the hydrogen- and methane-sensing performance of 2D ZnO nanowalls. they were directly grown on a glass substrate by thermal evaporation of zinc powder at 450 °C. The fabrication process did not use a metal catalyst or the pre-deposition of a ZnO seed layer on the substrate. The nanostructure consisted of interconnected ZnO nanowalls of 1.3 µm in length and approximately 60 nm in thickness, grown along the c-axis. To fabricate the gas sensor, Pd interdigitated electrodes were deposited onto the sample by e-beam evaporation with the use of a metal mask. The sensing investigation of ZnO nanowalls showed good response to 100–3000 ppm of both gases at 300 °C, but higher for methane. The good sensitivity and short response/recovery times were attributed to the ZnO nanowalls, which have a large surface to volume ratio that can favor the effective and fast adsorption/desorption of gas molecules.

Table 8 summarizes the gas-sensing properties of the above-discussed 2D ZnO-based gas sensors.

Table 8. 2D ZnO-based gas sensors.

Material	Gas	Temperature (°C)	Concentration (ppm)	Response	Response/Recovery Times (s)	Ref.
2D SnO_2/ZnO heterostructure	H_2S	100	5	120 [1]	-/513	[89]
ZnO nanowalls	Hydrogen	300	3000	350 [2]	-/-	[90]
ZnO nanowalls	Methane	300	3000	810 [2]	6/21 [3]	[91]

[1] Response R_a/R_g; [2] Response $(I_g - I_a)/I_a$ %; [3] Time at 67% signal variation.

3.6. Humidity

The monitoring of humidity is a significant issue in various applications including instrumentation, industrial process, agriculture, biology, and climatology. For this reason, numerous sorts of humidity sensors based on different materials and technologies have been fabricated and developed in recent years [92]. Humidity sensors based on semiconductor metal oxides have attracted considerable attention due to their ease of fabrication, clear operating mechanism, high sensing response, low cost, and portability. Among them, many different nanostructures of ZnO such as nanowires, nanorods, nanoparticles, and nanofibers have been proposed as high-performance relative humidity (RH) sensors [93–96]. Following the increased interest in the investigation of the sensing

properties of the 2D ZnO nanostructures, some works have been also devoted to the use of these materials as humidity sensors.

Tsai and Wang [97] investigated the effectiveness of using laterally oriented ZnO nanosheets grown by a hydrothermal method on a silicon substrate for RH sensing at room temperature. For the fabrication of the sensor, an Al-doped zinc oxide (AZO) thick film was sputtered on oxidized silicon substrates, then two Pt electrodes were deposited via an e-beam system onto the AZO layer. Finally, ZnO nanosheets were grown along the AZO sidewalls. The authors, investigating the sensing performance towards humidity from 96 to 12% RH, observed a response as high as $R_{12\%}/R_{96\%}$ = 220, excellent linear behavior in the whole range investigated, and short response/recovery times of 600s and 3 s, respectively (Figure 18a–d). Furthermore, the RH-sensing response of the proposed ZnO nanosheet-based sensor was as much as 100-fold higher than that of a ZnO-nanowire-based sensor (Figure 18e). they also investigated the selectivity to humidity in comparison to other gases such as hydrogen, ethanol, ammonia, and nitrogen dioxide (Figure 18f). The relatively low responses observed towards these gases were attributed to insufficient thermal energy at room temperature, which favors the response to humidity, therefore resulting in a high selectivity.

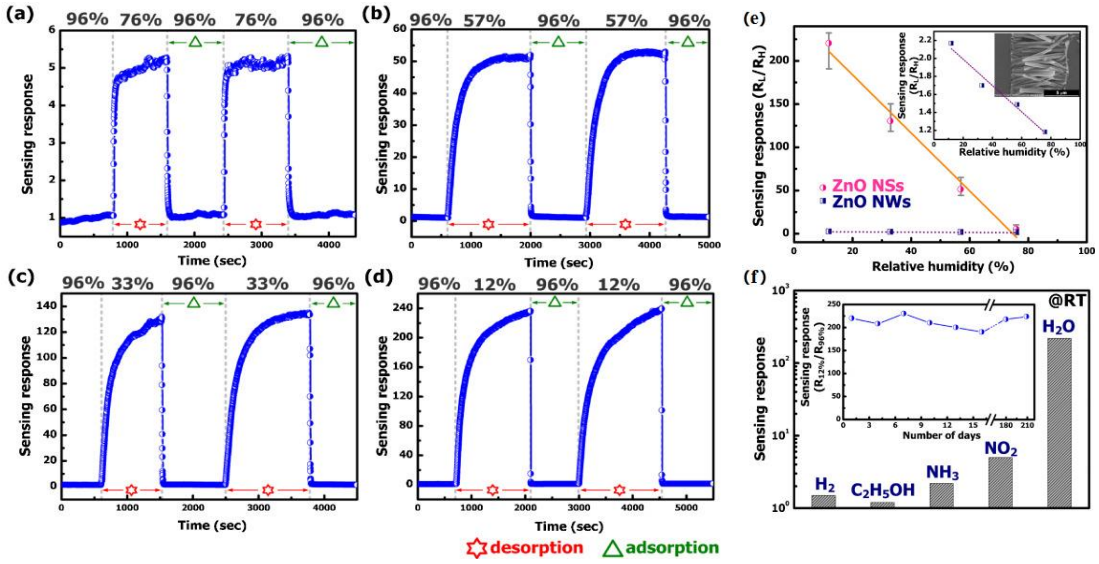

Figure 18. Dynamic responses of ZnO-nanosheet-based sensors in ambient air with RH variations (**a**) 96–76%, (**b**) 96–57%, (**c**) 96–33%, and (**d**) 96–12%; (**e**) calibration curves of ZnO nanosheets (NSs) and ZnO nanowire (NW) (inset)-based sensors at room temperature; (**f**) selectivity and long-term stability (inset) of ZnO-nanosheet-based sensor. Reprinted from [97] with permission from Elsevier.

Bu and Yang [98] synthesized, directly on a glass substrate, ZnO nanoflakes by a solvothermal method followed by an annealing at 550 °C for the complete transformation of zinc acetate precursors to zinc oxide. ZnO nanoflakes were approximately 1–2 µm in diameter and tilted on the glass substrate, providing a good coverage without visible voids. The sensor was finally fabricated by photolithography deposition of electrical contacts on the sensitive film. Comparing the response to humidity of ZnO nanoflakes with a conventional sputtered ZnO film, a faster response was obtained for the 2D nanostructures (10 s from 90 to 30% RH). The authors proposed that the enhancements in humidity sensor performance were due to an increase in the available surface area and the significant amount of defects such as Zn and O voids. However, the sensor showed a resistance ratio response from 30 to 90% RH of only R_{90}/R_{30} = 1.07, which is lower than other 2D ZnO-based humidity sensors. This may be due to the compact film prepared with respect to the vertically aligned ZnO nanostructures, which provide a higher specific surface area.

Modaresinezhad and Darbari [99] reported the use of a piezoelectric nanogenerator based on ZnO nanosheets as a room-temperature self-powered humidity sensor. It consisted of a sandwich structure where ZnO nanowalls were grown on an Al layer, which acted as the bottom ohmic contact, while an upper Ni/ZnO contact acted as the Schottky contact (Figure 19a). ZnO nanowalls consisted of nanosheets with a thickness of about 50 nm and average lateral size of about 2–5 μm, directly grown by the hydrothermal method on an Al thin film deposited on a glass substrate (Figure 19b). Then, exploiting both the piezoelectric and sensing properties of ZnO nanowalls, a self-powered, sensitive humidity sensor was developed. The authors, operating in both short circuit and open circuit, which monitored the current and voltage, respectively (Figure 19c,d), obtained an excellent sensitivity to humidity variation, with a response about 10 times higher than when the same materials were used as a resistive sensor. By optimizing the structure of the device, a fast response time of 70 s was also obtained. Moreover, it was suggested that the alteration of both voltage and current parameters provided two separate outputs usable as the fingerprint of humidity, which is helpful for the selectivity.

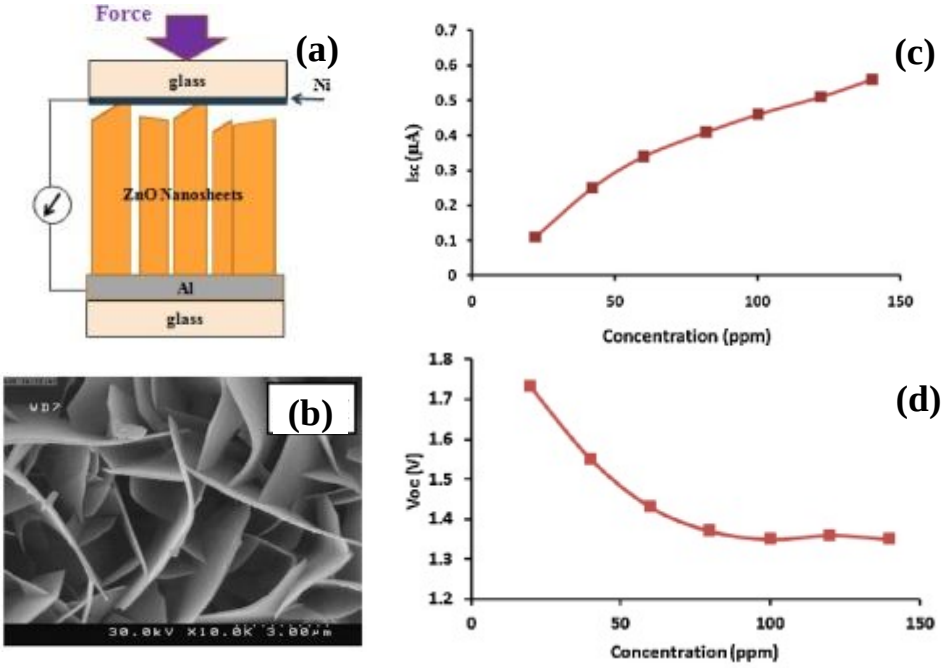

Figure 19. (**a**) Schematic structure of the fabricated sensor; (**b**) SEM image of the grown nanosheets; variation of (**c**) short-circuit current; and (**d**) open circuit voltage, versus changing humidity concentration at room temperature. Reprinted from [99] with permission from Elsevier.

4. Conclusions

In this paper a comprehensive review of many of the most interesting articles about gas sensors based on two-dimensional (2D) ZnO nanostructures has been made.

2D ZnO nanostructures have generally superior performance compared to other structures due to the high specific surface area conferred by the special aspect ratio. In particular, when these 2D materials are assembled to form three-dimensional hierarchical nanostructures such as nanoflowers, vertically aligned nanowalls and 1D/2D combined structures, the sensing performances are greatly improved. The self-arrangement of these nanostructures avoids the agglomeration of the material during the fabrication of the sensor, leading to a porous and open sensitive film; therefore, the typically high specific surface area of 2D nanostructures can be better exploited. Favoring the rapid diffusion of gases through the channels and the gas absorption on the surface of the material results in the improvement of sensitivity and dynamic response. It is worth noting that a greater number of absorbed molecules requires a longer desorption time, particularly if the working temperature is insufficient to

provide adequate energy to activate the desorption process of gas molecules from the material surface. Consequently, although many of the 2D ZnO nanostructures exhibit excellent sensitivity working at low temperatures, if the interaction between molecules and material is strong the sensors show long or incomplete recovery of the signal.

Many studies have shown how it is possible to control the synthesis in order to grow ZnO nanostructures with an unconventional growth direction of the crystals. This meant that, in addition to exploiting the typical high surface to volume ratio of 2D nanostructures, it has been possible to dispose of materials with specific exposed facets of the crystal. The experimental tests, where similar ZnO nanostructures but with different exposed facets were used, have shown that it is possible to tune the sensing properties towards specific substances, improving both the sensitivity and selectivity of the material. Some theoretical studies, carried out using DFT simulations, have also allowed us to explain these effects by investigating the reactivity of each exposed facet as well as the binding energies involved in the absorption of gaseous molecules. For instance, it was observed that the reactive (0001) facet easily absorbs oxygen species, which are primarily involved in the sensing mechanism towards different gases, on its surface. Unlike other exposed planes, which exhibit lower diffusivities towards specific molecules, they may improve the adsorption capability of these and thus the sensitivity and selectivity to specific gases. Theoretical simulation together with experimental results can be useful for understanding the adsorption behaviors of different gases on the various ZnO crystal facets in order to design various nanomaterials with tuned gas-sensing performance.

Acknowledgments: This work has been carried out under the framework of the project "Research & Mobility 2016" funded by the University of Messina.

Conflicts of Interest: The author declares no conflict of interest.

References

1. Liu, X.; Cheng, S.; Liu, H.; Hu, S.; Zhang, D.; Ning, H. A survey on gas sensing technology. *Sensors* **2012**, *12*, 9635–9665. [CrossRef] [PubMed]
2. Neri, G. First fifty years of chemoresistive gas sensors. *Chemosensors* **2015**, *3*, 1–20. [CrossRef]
3. Fine, G.F.; Cavanagh, L.M.; Afonja, A.; Binions, R. Metal oxide semi-conductor gas sensors in environmental monitoring. *Sensors* **2010**, *10*, 5469–5502. [CrossRef] [PubMed]
4. Patil, S.J.; Patil, A.V.; Dighavkar, C.G.; Thakare, K.S.; Borase, R.Y.; Nandre, S.J.; Deshpande, N.G.; Ahire, R.R. Semiconductor metal oxide compounds based gas sensors: A literature review. *Front. Mater. Sci.* **2015**, *9*, 14–37. [CrossRef]
5. Wang, C.; Yin, L.; Zhang, L.; Xiang, D.; Gao, R. Metal oxide gas sensors: Sensitivity and influencing factors. *Sensors* **2010**, *10*, 2088–2106. [CrossRef] [PubMed]
6. Arafat, M.M.; Dinan, B.; Akbar, S.A.; Haseeb, A.S.M.A. Gas sensors based on one dimensional nanostructured metal-oxides: A review. *Sensors* **2012**, *12*, 7207–7258. [CrossRef] [PubMed]
7. Galstyan, V.; Comini, E.; Ponzoni, A.; Sberveglieri, V.; Sberveglieri, G. ZnO quasi-1D nanostructures: Synthesis, modeling, and properties for applications in conductometric chemical sensors. *Chemosensors* **2016**, *4*, 6. [CrossRef]
8. Varghese, S.S.; Varghese, S.H.; Swaminathan, S.; Singh, K.K.; Mittal, V. Two-dimensional materials for sensing: Graphene and beyond. *Electronics* **2015**, *4*, 651–687. [CrossRef]
9. Gupta, A.; Sakthivel, T.; Seal, S. Recent development in 2D materials beyond graphene. *Prog. Mater. Sci.* **2015**, *73*, 44–126. [CrossRef]
10. Yang, W.; Gan, L.; Li, H.; Zhai, T. Two-dimensional layered nanomaterials for gas-sensing applications. *Inorg. Chem. Front.* **2016**, *3*, 433–451. [CrossRef]
11. Kaneti, Y.V.; Zhang, Z.; Yue, J.; Zakaria, Q.M.D.; Chen, C.; Jiang, X.; Yu, A. Crystal plane-dependent gas-sensing properties of zinc oxide nanostructures: Experimental and theoretical studies. *Phys. Chem. Chem. Phys.* **2014**, *16*, 11471–11480. [CrossRef] [PubMed]
12. Kim, H.-J.; Lee, J.-H. Highly sensitive and selective gas sensors using p-type oxide semiconductors: Overview. *Sens. Actuators B Chem.* **2014**, *192*, 607–627. [CrossRef]

13. Hjiri, M.; Mir, L.E.; Leonardi, S.G.; Pistone, A.; Mavilia, L.; Neri, G. Al-doped ZnO for highly sensitive CO gas sensors. *Sens. Actuators B Chem.* **2014**, *196*, 413–420. [CrossRef]
14. Fan, F.; Zhang, J.; Li, J.; Zhang, N.; Hong, R.; Deng, X.; Tang, P.; Li, D. Hydrogen sensing properties of Pt-Au bimetallic nanoparticles loaded on ZnO nanorods. *Sens. Actuators B Chem.* **2017**, *241*, 895–903. [CrossRef]
15. Kulandaisamy, A.J.; Reddy, J.R.; Srinivasan, P.; Babu, K.J.; Mani, G.K.; Shankar, P.; Rayappan, J.B.B. Room temperature ammonia sensing properties of ZnO thin films grown by spray pyrolysis: Effect of mg doping. *J. Alloys Compd.* **2016**, *688*, 422–429. [CrossRef]
16. Rambu, A.P.; Iftimie, N.; Nica, V.; Dobromir, M.; Tascu, S. Efficient methane detection by Co doping of ZnO thin films. *Superlattices Microstruct.* **2015**, *78*, 61–70. [CrossRef]
17. Wang, J.; Yang, J.; Han, N.; Zhou, X.; Gong, S.; Yang, J.; Hu, P.; Chen, Y. Highly sensitive and selective ethanol and acetone gas sensors based on modified ZnO nanomaterials. *Mater. Des.* **2017**, *121*, 69–76. [CrossRef]
18. Hjiri, M.; Mir, L.E.; Leonardi, S.G.; Donato, N.; Neri, G. CO and NO_2 selective monitoring by ZnO-based sensors. *Nanomaterials* **2013**, *3*, 357–369. [CrossRef] [PubMed]
19. Xiao, C.; Yang, T.; Chuai, M.; Xiao, B.; Zhang, M. Synthesis of ZnO nanosheet arrays with exposed (100) facets for gas sensing applications. *Phys. Chem. Chem. Phys.* **2016**, *18*, 325–330. [CrossRef] [PubMed]
20. Bai, S.; Hu, J.; Li, D.; Luo, R.; Chen, A.; Liu, C.C. Quantum-sized ZnO nanoparticles: Synthesis, characterization and sensing properties for NO_2. *J. Mater. Chem.* **2011**, *21*, 12288–12294. [CrossRef]
21. Gurav, K.V.; Gang, M.G.; Shin, S.W.; Patil, U.M.; Deshmukh, P.R.; Agawane, G.L.; Suryawanshi, M.P.; Pawar, S.M.; Patil, P.S.; Lokhande, C.D.; et al. Gas sensing properties of hydrothermally grown ZnO nanorods with different aspect ratios. *Sens. Actuators B Chem.* **2014**, *190*, 439–445. [CrossRef]
22. Cao, Y.; Zou, X.; Wang, X.; Qian, J.; Bai, N.; Li, G.-D. Effective detection of trace amount of explosive nitro-compounds by ZnO nanofibers with hollow structure. *Sens. Actuators B Chem.* **2016**, *232*, 564–570. [CrossRef]
23. Huang, B.; Zhao, C.; Zhang, M.; Zhang, Z.; Xie, E.; Zhou, J.; Han, W. Doping effect of In_2O_3 on structural and ethanol-sensing characteristics of ZnO nanotubes fabricated by electrospinning. *Appl. Surf. Sci.* **2015**, *349*, 615–621. [CrossRef]
24. Liu, X.; Zhang, J.; Wang, L.; Yang, T.; Guo, X.; Wu, S.; Wang, S. 3D hierarchically porous ZnO structures and their functionalization by au nanoparticles for gas sensors. *J. Mater. Chem.* **2011**, *21*, 349–356. [CrossRef]
25. Liu, Y.; Liu, H.; Zhang, Q.; Li, T. Adjusting the proportions of {0001} facets and high-index facets of ZnO hexagonal prisms and their photocatalytic activity. *RSC Adv.* **2017**, *7*, 3515–3520. [CrossRef]
26. Liu, X.; Ye, L.; Liu, S.; Li, Y.; Ji, X. Photocatalytic reduction of CO_2 by ZnO micro/nanomaterials with different morphologies and ratios of {0001} facets. *Sci. Rep.* **2016**, *6*, 38474. [CrossRef] [PubMed]
27. Chang, J.; Ahmad, M.; Wlodarski, W.; Waclawik, E. Self-assembled 3D ZnO porous structures with exposed reactive {0001} facets and their enhanced gas sensitivity. *Sensors* **2013**, *13*, 8445–8460. [CrossRef] [PubMed]
28. Kaneti, Y.V.; Yue, J.; Jiang, X.; Yu, A. Controllable synthesis of ZnO nanoflakes with exposed $(10\bar{1}0)$ for enhanced gas sensing performance. *J. Phys. Chem. C* **2013**, *117*, 13153–13162. [CrossRef]
29. Liu, J.; Chen, X.; Wang, W.; Liu, Y.; Huang, Q.; Guo, Z. Self-assembly of [1010] grown ZnO nanowhiskers with exposed reactive (0001) facets on hollow spheres and their enhanced gas sensitivity. *CrystEngComm* **2011**, *13*, 3425–3431. [CrossRef]
30. Xiao, Y.; Lu, L.; Zhang, A.; Zhang, Y.; Sun, L.; Huo, L.; Li, F. Highly enhanced acetone sensing performances of porous and single crystalline ZnO nanosheets: High percentage of exposed (100) facets working together with surface modification with pd nanoparticles. *ACS Appl. Mater. Interfaces* **2012**, *4*, 3797–3804. [CrossRef] [PubMed]
31. Han, X.; Jin, M.; Xie, S.; Kuang, Q.; Jiang, Z.; Jiang, Y.; Xie, Z.; Zheng, L. Synthesis of tin dioxide octahedral nanoparticles with exposed high-energy {221} facets and enhanced gas-sensing properties. *Angew. Chem. Int. Ed.* **2009**, *48*, 9180–9183. [CrossRef] [PubMed]
32. Han, X.; Han, X.; Li, L.; Wang, C. Controlling the morphologies of WO_3 particles and tuning the gas sensing properties. *New J. Chem.* **2012**, *36*, 2205–2208. [CrossRef]
33. Yang, Y.; Liang, Y.; Wang, G.; Liu, L.; Yuan, C.; Yu, T.; Li, Q.; Zeng, F.; Gu, G. Enhanced gas-sensing properties of the hierarchical TiO_2 hollow microspheres with exposed high-energy {001} crystal facets. *ACS Appl. Mater. Interfaces* **2015**, *7*, 24902–24908. [CrossRef] [PubMed]
34. Xu, J.; Xue, Z.; Qin, N.; Cheng, Z.; Xiang, Q. The crystal facet-dependent gas sensing properties of ZnO nanosheets: Experimental and computational study. *Sens. Actuators B Chem.* **2017**, *242*, 148–157. [CrossRef]

35. Kumar, R.; Al-Dossary, O.; Kumar, G.; Umar, A. Zinc oxide nanostructures for NO_2 gas-sensor applications: A review. *Nano-Micro Lett.* **2015**, *7*, 97–120. [CrossRef]
36. Wang, Z.L. Zinc oxide nanostructures: Growth, properties and applications. *J. Phys. Condens. Matter* **2004**, *16*, 829–858. [CrossRef]
37. Liu, J.; Hu, Z.-Y.; Peng, Y.; Huang, H.-W.; Li, Y.; Wu, M.; Ke, X.-X.; Tendeloo, G.V.; Su, B.-L. 2D ZnO mesoporous single-crystal nanosheets with exposed {0001} polar facets for the depollution of cationic dye molecules by highly selective adsorption and photocatalytic decomposition. *Appl. Catal. B Environ.* **2016**, *181*, 138–145. [CrossRef]
38. Zhang, X.L.; Qiao, R.; Qiu, R.; Kim, J.C.; Kang, Y.S. Fabrication of hierarchical ZnO nanostructures via a surfactant-directed process. *Cryst. Growth Des.* **2009**, *9*, 2906–2910. [CrossRef]
39. Breedon, M.; Spencer, M.J.S.; Yarovsky, I. Adsorption of NO and NO_2 on the ZnO surface: A dft study. *Surf. Sci.* **2009**, *603*, 3389–3399. [CrossRef]
40. Breedon, M.; Spencer, M.J.S.; Yarovsky, I. Adsorption of NO_2 on oxygen deficient ZnO $(2\bar{1}\bar{1}0)$ for gas sensing applications: A DFT study. *J. Phys. Chem. C* **2010**, *114*, 16603–16610. [CrossRef]
41. Prades, J.D.; Cirera, A.; Morante, J.R. Ab initio calculations of NO_2 and SO_2 chemisorption onto non-polar ZnO surfaces. *Sens. Actuators B Chem.* **2009**, *142*, 179–184. [CrossRef]
42. Yuan, Q.; Zhao, Y.-P.; Li, L.; Wang, T. Ab initio study of ZnO-based gas-sensing mechanisms: Surface reconstruction and charge transfer. *J. Phys. Chem. C* **2009**, *113*, 6107–6113. [CrossRef]
43. Kansal, A. Sources and reactivity of NMHCs and VOCs in the atmosphere: A review. *J. Hazard. Mater.* **2009**, *166*, 17–26. [CrossRef] [PubMed]
44. Bartzis, J.; Wolkoff, P.; Stranger, M.; Efthimiou, G.; Tolis, E.I.; Maes, F.; Nørgaard, A.W.; Ventura, G.; Kalimeri, K.K.; Goelen, E.; et al. On organic emissions testing from indoor consumer products' use. *J. Hazard. Mater.* **2015**, *285*, 37–45. [CrossRef] [PubMed]
45. Leidinger, M.; Sauerwald, T.; Conrad, T.; Reimringer, W.; Ventura, G.; Schütze, A. Selective detection of hazardous indoor VOCs using metal oxide gas sensors. *Procedia Eng.* **2014**, *87*, 1449–1452. [CrossRef]
46. Mirzaei, A.; Leonardi, S.G.; Neri, G. Detection of hazardous volatile organic compounds (VOCs) by metal oxide nanostructures-based gas sensors: A review. *Ceram. Int.* **2016**, *42*, 15119–15141. [CrossRef]
47. Xie, X.; Wang, X.; Tian, J.; Song, X.; Wei, N.; Cui, H. Growth of porous ZnO single crystal hierarchical architectures with ultrahigh sensing performances to ethanol and acetone gases. *Ceram. Int.* **2017**, *43*, 1121–1128. [CrossRef]
48. Zhang, L.; Zhao, J.; Lu, H.; Li, L.; Zheng, J.; Li, H.; Zhu, Z. Facile synthesis and ultrahigh ethanol response of hierarchically porous ZnO nanosheets. *Sens. Actuators B Chem.* **2012**, *161*, 209–215. [CrossRef]
49. Liu, Y.; Dong, J.; Hesketh, P.J.; Liu, M. Synthesis and gas sensing properties of ZnO single crystal flakes. *J. Mater. Chem.* **2005**, *15*, 2316–2320. [CrossRef]
50. Zhang, Y.; Liu, C.; Gong, F.; Jiu, B.; Li, F. Large scale synthesis of hexagonal simonkolleit nanosheets for ZnO gas sensors with enhanced performances. *Mater. Lett.* **2017**, *186*, 7–11. [CrossRef]
51. Chen, Z.; Lin, Z.; Xu, M.; Hong, Y.; Li, N.; Fu, P.; Chen, Z. Effect of gas sensing properties by Sn-Rh codoped ZnO nanosheets. *Electron. Mater. Lett.* **2016**, *12*, 343–349. [CrossRef]
52. Fan, F.; Tang, P.; Wang, Y.; Feng, Y.; Chen, A.; Luo, R.; Li, D. Facile synthesis and gas sensing properties of tubular hierarchical ZnO self-assembled by porous nanosheets. *Sens. Actuators B Chem.* **2015**, *215*, 231–240. [CrossRef]
53. Yu, L.-M.; Guo, F.; Liu, Z.-Y.; Liu, S.; Yang, B.; Yin, M.-L.; Fan, X.-H. Facile synthesis of three dimensional porous ZnO films with mesoporous walls and gas sensing properties. *Mater. Charact.* **2016**, *112*, 224–228. [CrossRef]
54. Alenezi, M.R.; Henley, S.J.; Emerson, N.G.; Silva, S.R.P. From 1D and 2D ZnO nanostructures to 3D hierarchical structures with enhanced gas sensing properties. *Nanoscale* **2014**, *6*, 235–247. [CrossRef] [PubMed]
55. Al-Hadeethi, Y.; Umar, A.; Al-Heniti, S.H.; Kumar, R.; Kim, S.H.; Zhang, X.; Raffah, B.M. 2D Sn-doped ZnO ultrathin nanosheet networks for enhanced acetone gas sensing application. *Ceram. Int.* **2017**, *43*, 2418–2423. [CrossRef]
56. Fan, H.; Jia, X. Selective detection of acetone and gasoline by temperature modulation in zinc oxide nanosheets sensors. *Solid State Ion.* **2011**, *192*, 688–692. [CrossRef]

57. Wen, W.; Wu, J.-M.; Wang, Y.-D. Large-size porous ZnO flakes with superior gas-sensing performance. *Appl. Phys. Lett.* **2012**, *100*, 262111. [CrossRef]
58. Behera, B.; Chandra, S. An innovative gas sensor incorporating ZnO-CuO nanoflakes in planar MEMS technology. *Sens. Actuators B Chem.* **2016**, *229*, 414–424. [CrossRef]
59. Guo, W. Design of gas sensor based on Fe-doped ZnO nanosheet-spheres for low concentration of formaldehyde detection. *J. Electrochem. Soc.* **2016**, *163*, B517–B525. [CrossRef]
60. Chen, Z.-W.; Hong, Y.-Y.; Lin, Z.-D.; Liu, L.-M.; Zhang, X.-W. Enhanced formaldehyde gas sensing properties of ZnO nanosheets modified with graphene. *Electron. Mater. Lett.* **2017**, *13*, 270–276. [CrossRef]
61. Zhang, S.-L.; Lim, J.-O.; Huh, J.-S.; Noh, J.-S.; Lee, W. Two-step fabrication of ZnO nanosheets for high-performance VOCs gas sensor. *Curr. Appl. Phys.* **2013**, *13*, S156–S161. [CrossRef]
62. Guo, W.; Fu, M.; Zhai, C.; Wang, Z. Hydrothermal synthesis and gas-sensing properties of ultrathin hexagonal ZnO nanosheets. *Ceram. Int.* **2014**, *40*, 2295–2298. [CrossRef]
63. Chen, Y.; Shen, Z.; Jia, Q.; Zhao, J.; Zhao, Z.; Ji, H. A CuO-ZnO nanostructured p-n junction sensor for enhanced n-butanol detection. *RSC Adv.* **2016**, *6*, 2504–2511. [CrossRef]
64. Wang, L.; Wang, S.; Zhang, H.; Wang, Y.; Yang, J.; Huang, W. Au-functionalized porous ZnO microsheets and their enhanced gas sensing properties. *New J. Chem.* **2014**, *38*, 2530–2537. [CrossRef]
65. Huang, J.; Wu, Y.; Gu, C.; Zhai, M.; Yu, K.; Yang, M.; Liu, J. Large-scale synthesis of flowerlike ZnO nanostructure by a simple chemical solution route and its gas-sensing property. *Sens. Actuators B Chem.* **2010**, *146*, 206–212. [CrossRef]
66. Gu, C.; Huang, H.; Huang, J.; Jin, Z.; Zheng, H.; Liu, N.; Li, M.; Liu, J.; Meng, F. Chlorobenzene sensor based on Pt-decorated porous single-crystalline ZnO nanosheets. *Sens. Actuators A Phys.* **2016**, *252*, 96–103. [CrossRef]
67. Jing, Z.; Zhan, J. Fabrication and gas-sensing properties of porous ZnO nanoplates. *Adv. Mater.* **2008**, *20*, 4547–4551. [CrossRef]
68. Zhang, L.; Zhao, J.; Lu, H.; Li, L.; Zheng, J.; Zhang, J.; Li, H.; Zhu, Z. Highly sensitive and selective dimethylamine sensors based on hierarchical ZnO architectures composed of nanorods and nanosheet-assembled microspheres. *Sens. Actuators B Chem.* **2012**, *171–172*, 1101–1109. [CrossRef]
69. Tonezzer, M.; Dang, T.T.L.; Bazzanella, N.; Nguyen, V.H.; Iannotta, S. Comparative gas-sensing performance of 1D and 2D ZnO nanostructures. *Sens. Actuators B Chem.* **2015**, *220*, 1152–1160. [CrossRef]
70. Kaneti, Y.V.; Zhang, X.; Liu, M.; Yu, D.; Yuan, Y.; Aldous, L.; Jiang, X. Experimental and theoretical studies of gold nanoparticle decorated zinc oxide nanoflakes with exposed $\{10\bar{1}0\}$ facets for butylamine sensing. *Sens. Actuators B Chem.* **2016**, *230*, 581–591. [CrossRef]
71. Yu, L.; Wei, J.; Luo, Y.; Tao, Y.; Lei, M.; Fan, X.; Yan, W.; Peng, P. Dependence of Al^{3+} on the growth mechanism of vertical standing ZnO nanowalls and their NO_2 gas sensing properties. *Sens. Actuators B Chem.* **2014**, *204*, 96–101. [CrossRef]
72. Yu, L.; Guo, F.; Liu, S.; Yang, B.; Jiang, Y.; Qi, L.; Fan, X. Both oxygen vacancies defects and porosity facilitated NO_2 gas sensing response in 2D ZnO nanowalls at room temperature. *J. Alloy. Compd.* **2016**, *682*, 352–356. [CrossRef]
73. Chen, M.; Wang, Z.; Han, D.; Gu, F.; Guo, G. Porous ZnO polygonal nanoflakes: Synthesis, use in high-sensitivity NO_2 gas sensor, and proposed mechanism of gas sensing. *J. Phys. Chem. C* **2011**, *115*, 12763–12773. [CrossRef]
74. Wang, J.; Li, X.; Xia, Y.; Komarneni, S.; Chen, H.; Xu, J.; Xiang, L.; Xie, D. Hierarchical ZnO nanosheet-nanorod architectures for fabrication of poly(3-hexylthiophene)/ZnO hybrid NO_2 sensor. *ACS Appl. Mater. Interfaces* **2016**, *8*, 8600–8607. [CrossRef] [PubMed]
75. Mun, Y.; Park, S.; An, S.; Lee, C.; Kim, H.W. NO_2 gas sensing properties of Au-functionalized porous ZnO nanosheets enhanced by UV irradiation. *Ceram. Int.* **2013**, *39*, 8615–8622. [CrossRef]
76. Wei, S.; Yu, Y.; Zhou, M. CO gas sensing of Pd-doped ZnO nanofibers synthesized by electrospinning method. *Mater. Lett.* **2010**, *64*, 2284–2286. [CrossRef]
77. Arunkumar, S.; Hou, T.; Kim, Y.-B.; Choi, B.; Park, S.H.; Jung, S.; Lee, D.-W. Au decorated ZnO hierarchical architectures: Facile synthesis, tunable morphology and enhanced CO detection at room temperature. *Sens. Actuators B Chem.* **2017**, *243*, 990–1001. [CrossRef]
78. Hjiri, M.; Mir, L.; Leonardi, S.G. Synthesis, characterization and sensing properties of AZO and IZO nanomaterials. *Chemosensors* **2014**, *2*, 121–130. [CrossRef]

79. Jones, D.R.; Maffeïs, T.G.G. Analysis of the kinetics of surface reactions on a zinc oxide nanosheet-based carbon monoxide sensor using an Eley-Rideal model. *Sens. Actuators B Chem.* **2015**, *218*, 16–24. [CrossRef]
80. Zeng, Y.; Qiao, L.; Bing, Y.; Wen, M.; Zou, B.; Zheng, W.; Zhang, T.; Zou, G. Development of microstructure CO sensor based on hierarchically porous ZnO nanosheet thin films. *Sens. Actuators B Chem.* **2012**, *173*, 897–902. [CrossRef]
81. Chang, S.-P.; Wen, C.-H.; Chang, S.-J. Two-dimensional ZnO nanowalls for gas sensor and photoelectrochemical applications. *Electron. Mater. Lett.* **2014**, *10*, 693–697. [CrossRef]
82. Chatterjee, B.; Bandyopadhyay, A. Development of zinc oxide sensors for detecting ammonia gas in the ambient air: A critical short review. *Environ. Q. Manag.* **2016**, *26*, 89–105. [CrossRef]
83. Sarala Devi, G.; Bala Subrahmanyam, V.; Gadkari, S.C.; Gupta, S.K. NH_3 gas sensing properties of nanocrystalline ZnO based thick films. *Anal. Chim. Acta* **2006**, *568*, 41–46. [CrossRef] [PubMed]
84. Mani, G.K.; Rayappan, J.B.B. A highly selective room temperature ammonia sensor using spray deposited zinc oxide thin film. *Sens. Actuators B Chem.* **2013**, *183*, 459–466. [CrossRef]
85. Mani, G.K.; Rayappan, J.B.B. A highly selective and wide range ammonia sensor—Nanostructured ZnO:Co thin film. *Mater. Sci. Eng. B* **2015**, *191*, 41–50. [CrossRef]
86. Liu, J.; Guo, Z.; Meng, F.; Luo, T.; Li, M.; Liu, J. Novel porous single-crystalline ZnO nanosheets fabricated by annealing ZnS(en) 0.5 (en = ethylenediamine) precursor. Application in a gas sensor for indoor air contaminant detection. *Nanotechnology* **2009**, *20*, 125501. [CrossRef] [PubMed]
87. Nguyen, D.D.; Do, D.T.; Vu, X.H.; Dang, D.V.; Nguyen, D.C. ZnO nanoplates surfaced-decorated by WO_3 nanorods for NH_3 gas sensing application. *Adv. Nat. Sci. Nanosci. Nanotechnol.* **2016**, *7*, 015004. [CrossRef]
88. Li, Y.; Jiao, M.; Yang, M. In-situ grown nanostructured ZnO via a green approach and gas sensing properties of polypyrrole/ZnO nanohybrids. *Sens. Actuators B Chem.* **2017**, *238*, 596–604. [CrossRef]
89. Fu, D.; Zhu, C.; Zhang, X.; Li, C.; Chen, Y. Two-dimensional net-like SnO_2/ZnO heteronanostructures for high-performance H_2S gas sensor. *J. Mater. Chem. A* **2016**, *4*, 1390–1398. [CrossRef]
90. Chen, T.P.; Chang, S.P.; Chang, S.J. Fabrication of ZnO nanowall-based hydrogen gas nanosensor. *Adv. Mater. Res.* **2013**, *684*, 21–25. [CrossRef]
91. Chen, T.-P.; Chang, S.-P.; Hung, F.-Y.; Chang, S.-J.; Hu, Z.-S.; Chen, K.-J. Simple fabrication process for 2D ZnO nanowalls and their potential application as a methane sensor. *Sensors* **2013**, *13*, 3941–3950. [CrossRef] [PubMed]
92. Farahani, H.; Wagiran, R.; Hamidon, M.N. Humidity sensors principle, mechanism, and fabrication technologies: A comprehensive review. *Sensors* **2014**, *14*, 7881–7939. [CrossRef] [PubMed]
93. Wan, Q.; Li, Q.H.; Chen, Y.J.; Wang, T.H.; He, X.L.; Gao, X.G.; Li, J.P. Positive temperature coefficient resistance and humidity sensing properties of Cd-doped ZnO nanowires. *Appl. Phys. Lett.* **2004**, *84*, 3085–3087. [CrossRef]
94. Zhang, Y.; Yu, K.; Jiang, D.; Zhu, Z.; Geng, H.; Luo, L. Zinc oxide nanorod and nanowire for humidity sensor. *Appl. Surf. Sci.* **2005**, *242*, 212–217. [CrossRef]
95. Erol, A.; Okur, S.; Comba, B.; Mermer, Ö.; Arıkan, M.Ç. Humidity sensing properties of ZnO nanoparticles synthesized by sol-gel process. *Sens. Actuators B Chem.* **2010**, *145*, 174–180. [CrossRef]
96. Wang, W.; Li, Z.; Liu, L.; Zhang, H.; Zheng, W.; Wang, Y.; Huang, H.; Wang, Z.; Wang, C. Humidity sensor based on LiCl-doped ZnO electrospun nanofibers. *Sens. Actuators B Chem.* **2009**, *141*, 404–409. [CrossRef]
97. Tsai, F.-S.; Wang, S.-J. Enhanced sensing performance of relative humidity sensors using laterally grown ZnO nanosheets. *Sens. Actuators B Chem.* **2014**, *193*, 280–287. [CrossRef]
98. Bu, I.Y.Y.; Yang, C.-C. High-performance ZnO nanoflake moisture sensor. *Superlattices Microstruct.* **2012**, *51*, 745–753. [CrossRef]
99. Modaresinezhad, E.; Darbari, S. Realization of a room-temperature/self-powered humidity sensor, based on ZnO nanosheets. *Sens. Actuators B Chem.* **2016**, *237*, 358–366. [CrossRef]